Evaluation of Cirrus Cloud Properties Derived From MODIS Data Using Cloud Properties Derived From Ground-Based Observations Collected at the ARM SGP Site

Gerald G. Mace and Yuying Zhang
University of Utah
Steven Platnick and Michael D. King
NASA Goddard Space Flight Center
Patrick Minnis
NASA Langley Research Center
Ping Yang
Texas A and M

Journal of Applied Meteorology
Manuscript submitted November 10, 2003
Revised June, 2004

Corresponding Author Address:
Gerald Mace
Department of Meteorology
University of Utah
135S 1460E Rm 819 (819 WBB)
Salt Lake City, Utah 84112-0110
email: mace@met.utah.edu

Abstract: The Moderate Resolution Imaging Spectroradiometer (MODIS) on board the NASA Terra satellite has been collecting global data since March 2000 and on the Aqua satellite since June 2002. In this paper we compare cirrus cloud properties derived from ground-based remote sensing data with similar cloud properties derived from MODIS data on Terra. In order to improve the space-time correlation between the satellite and ground-based observations, we use data from a wind profiler to define the cloud advective streamline along which the comparisons are made. In this paper we examine approximately two dozen cases of cirrus and explore a statistical approach to the comparison that relaxes the requirement that clouds occur over the ground-based instruments during the overpass instant. The statistical comparison includes 168 cloudy MODIS overpasses of the SGP region and approximately 300 hours of ground-based cirrus observations. The physical and radiative properties of cloud layers are derived from MODIS data separately by the MODIS Atmospheres team and the Clouds and the Earth's Radiant Energy System (CERES) Science Team using multiwavelength reflected solar and emitted thermal radiation measurements. Using two ground-based cloud property retrieval algorithms and the two MODIS algorithms, we show a positive correlation in the effective particle size, the optical thickness, the ice water path, and the cloud top pressure between the various methods, although sometimes there are significant biases. Classifying the clouds by optical thickness, we demonstrate that the regionally averaged cloud properties derived from MODIS are similar to those diagnosed from the ground. Due to a conservative approach toward identifying thin cirrus pixels over this region, the area-averaged cloud properties derived from the MODIS Atmospheres MOD06 product tend to be biased slightly toward the optically thicker pixels. This bias tendency has implications for model validation and parameterization development applied to thin cirrus retrieved over SGP-like land surfaces. We also find a persistent bias in the reported cloud tops of thin cirrus with both satellite algorithms reporting cloud top several hundred meters less than that reported by the cloud radar. We conclude overall, however, that the MODIS retrieval algorithms characterize with reasonably accuracy the properties of thin cirrus over this region.

1. Introduction

Cirrus clouds are globally distributed and are composed almost exclusively of nonspherical ice crystals with an annual global and local frequency of occurrence of about 30% (i.e., Wylie et al. 1989; Wylie et al. 1994; Rossow and Schiffer 1999). Satellite imagery shows that large cirrus systems modify the planetary radiation budget by increasing albedo and reducing infrared emission (Liou et al. 1986). Cirrus clouds not only play a significant role in the energy budget of the Earth-atmosphere system by means of their effects on the transfer of radiant energy through the atmosphere, but are also important as a vital link in the hydrological cycle (Stephens et al. 1990; Webster 1994). Given their importance (Lynch et al. 2002), it is necessary to accurately characterize cirrus clouds in models of the global climate (GCMs). However, given the extreme variability of cirrus microphysical properties and the interaction between solar radiation and the nonspherical particles composing cirrus clouds, their role in the climate system is not yet fully understood nor accurately characterized in models.

High level cirrus tend to have low concentrations of large particles relative to most clouds and are, therefore, typically optically thin and gray in the thermal IR spectrum (Ackerman et al. 1988). It has been recognized observationally and through numerical simulation that the influence of optically thin cirrus (defined as layers with infrared emittance less than 1) on the radiation field of the earth-atmosphere system, and hence on weather and climate components of the general circulation, depends on both the solar and thermal IR radiative properties. The radiative properties, in turn, are modulated by the physical composition of the cloud (ice water content, particle size, particle shape, and particle concentration) and the physical location of the layer in the atmosphere. In order to place the relevance and importance of cirrus composition, structure, and radiative properties into a global perspective and thereby improve the parameterization of cirrus clouds in GCMs, collections of analysis products including statistical distributions of fundamental cirrus cloud properties are required. Compiling these fundamental data will facilitate investigation of the influence of cirrus clouds on the thermodynamics and dynamics of the atmosphere, and ultimately lead to improved representation of clouds in climate models. Of particular importance in this respect is the need to characterize

simultaneously the relationship between the dynamics resolved by a large scale model, the subgridscale turbulence that ultimately maintains cloud elements, and the ice mass and particle sizes that evolve within these environments (Mace et al. 2001).

Present uncertainties in cloud parameterizations can be directly linked to the current scarcity of quantitative cloud property observations. In order to build a long term global data set, NASA's EOS (Earth Observing System) project launched its first spacecraft (Terra) on 18 December 1999 (King and Herring 2000). The Moderate Resolution Imaging Spectroradiometer (MODIS; Platnick et al. 2003; King et al. 2003; modis.gsfc.nasa.gov) is uniquely designed with wide spectral range, high spatial and spectral resolution, and near daily global coverage. Upwelling radiation in several narrow spectral channels at a resolution of 1 km in a 2300 km swath under the satellite track is measured by MODIS and converted into cloud properties using various algorithms (King et al. 1992, 1997, 2003; Platnick et al. 2003; Minnis et al. 1995, 1998, 2002). Due to the complex physical processes that relate the retrieved parameters to the upwelling radiances, the error characteristics of the retrievals need to be thoroughly understood before the retrieval results can be used quantitatively to improve our understanding of the role of cirrus in the climate system or to use this knowledge to develop cloud parameterizations for models. The two types of validation approaches expressed in the EOS ATBD (Algorithm Theoretical Basis Document) validation documents are the use of in situ aircraft in short term IOPs (Intensive Operational Periods) and the use of permanent observational facilities to perform validation over a long time period. In this paper we directly use the latter technique while the former is addressed in an indirect sense by first establishing the credibility of the ground-based measurements with in situ aircraft data (Appendix A).

Given the fine scale variability of most cloud systems (including cirrus), there is typically an extreme mismatch between the scales represented by in situ cloud observations collected from aircraft platforms and scales associated with spatially averaged satellite observations. This disparity applies not only to the horizontal dimensions but also to the vertical dimension since the information from solar reflected radiances comprise a non-linear weighting of the cloud properties of individual layers. Since it would take significant time to observationally characterize the volume over

which a satellite pixel is relevant, evolution of the cloud system will generally result in temporal changes that exacerbate the disparity. However, regardless of the problems that are inherent to the use of aircraft data in satellite cloud property validation, data collected *in situ* remain a valuable source of collaborative measurements and satellite-derived cloud properties should, ultimately, be traceable back to this sort of ground truth. In order to effectively make this quantitative connection between in situ data and pixel scale retrieved quantities, we use a bootstrapping method where the aircraft data are first compared to the results of cloud property retrieval algorithms applied to ground-based measurements (Mace et al. 2002; Dong and Mace 2003) and the ground-based results are then compared to those derived from satellites (Zhang 2002). The ground-based remote sensing measurements serve as an intermediate observational scale between the satellite pixel and the in situ observations. Since ground-based retrievals can be more easily validated against aircraft data, our goal is to essentially link satellite retrievals to the *in situ* measurements in this way. This approach has additional benefits. For instance, since ground-based instruments can be operated more routinely than can aircraft, we are able to create a statistically significant comparison data set in a shorter period of time and at less cost.

A proper validation of remotely sensed cloud properties would require enough cloud events to statistically characterize the bias and RMS (Root Mean Square) between the aircraft data and the ground-based data and between the ground-based data and the satellite. This has not yet been accomplished, however. The necessary aircraft data collected in coincidence with ground-based remote sensors simply do not exist, although we use much of what is available, as shown in Appendix A. Compiling the necessary number of MODIS coincidences with the ground-based remote sensors simply requires time, and the number of events is growing. In this paper, our goal is to illustrate our methodological approach for building a reasonable space-time correlated comparison between the ground-based results and cloud properties derived from MODIS data, as well as to present a comparison of a number of thin cirrus events. We also demonstrate a statistical approach to validation that measures whether relationships between certain cloud properties are similar between the ground-based and space-based retrievals. In any comparison of cirrus cloud particle sizes, a careful accounting must be made of the

differences in the definitions of particle size. Appendix B explores this issue for the algorithms used here.

2. Comparison Technique

We use two ground-based retrieval algorithms to compare with satellite-derived cirrus cloud properties. In this section we illustrate the use of an algorithm that relies on radar reflectivity and Doppler velocity (hereafter referred to as the Z-Velocity algorithm; Mace et al. 2002). The technique is applied to the ground-based data collected by the MMCR (Millimeter Cloud Radar; Moran et al. 1998) at the ARM sites. Concentrating on the capacity of the moments of the Doppler spectrum to provide information suitable for retrieving the microphysical properties of cirrus clouds, this algorithm uses the zeroth and first moments of the Doppler spectrum (radar reflectivity and mean Doppler velocity) to retrieve the cloud particle size distribution. This technique uses only measurements from the MMCR to retrieve the cloud properties, so it provides certain practical advantages compared to those requiring multiple instruments. An advantage of this technique over the Z-Radiance approach described in Appendix A and used in the next section is that the Z-Velocity algorithm has much higher (36 s) temporal resolution and provides vertically resolved cloud properties. It can also be applied without requiring the layer to be optically thin and observable without the presence of lower level clouds. However, the approach has significant limitations since in only a relatively small number of situations can the vertical air motion be reliably separated from the particle motions using a statistical technique (Mace et al. 2002).

Since the satellite observations represent a single moment in time over an area and the ARM data provide a time series from a single location, we improve the space-time correlation between the observations by using data from the Lamont 404 MHz NOAA wind profiler (36.6N 97.5W; 11 Km from the SGP ARM site). Using data from the Lamont profiler averaged over the depth of the cloud layer as observed by the MMCR, we define a streamline along which the observed cloud has passed in the 60 minute period centered on the satellite overpass (30 minutes before and 30 minutes after the overpass). Data are extracted from the MODIS-derived cloud products on either side of a 30 km wide streamline to create statistics of the cloud properties that would pass near the

SGP site. While the approach has obvious advantages, an assumption of stationarity in the cloud field properties during the 30 minute advection period from the SGP site does not always hold and individual features that exist within the cloud field do not always pass over the cloud radar. However, this approach does lead to more robust comparisons in many cases since it allows for comparison of meaningful cloud field statistics that respond more to the slowly varying large scale dynamics rather than the more rapidly varying updrafts and downdrafts that maintain individual cloud elements.

As an example, Terra passed over the ARM SGP site at 17:35:57 UTC with a view zenith angle of 1.3° on 6 March 2001 (Figure 1). Figure 2 shows the wind profile at Lamont on 6 March, 2001. After tracking approximately 45 km upstream and downstream of the ARM site to represent approximately 1 hour of ground data centered on the overpass, there are 7062 MODIS pixels to compare with the ground-based observations.

The operational pixel-level MODIS cloud product is archived under the file designation MOD06 (Platnick et al. 2003; King et al. 2003), and will be referred to as such throughout this paper. This product chooses the default cloud particle effective radius to be the one retrieved using the 2.1 μm MODIS band (though information for separate retrievals using the 1.6 and 3.7 μm bands are also available in the archived files). The MOD06 data used in the comparisons are collection 4; a designation that refers to the heritage of the algorithms used in the data processing of the MODIS radiances. The frequency distributions of selected cloud properties from MOD06 and those from the corresponding MMCR retrieval are displayed in Figure 3.

The cloud particle size compared here and in the remainder of the paper is the effective radius as defined by the MOD06 retrieval algorithm to be proportional to the ratio of the volume of ice to the projected area (specifically r_e=3/4*V/A) of the particle size spectrum where the geometric quantities are derived from a combination of various particle habits that depend on effective radius (Platnick et al. 2003). The forward radiative transfer computation used in the MOD06 retrieval algorithm assumes plates, hollow columns, bullet rosettes, and aggregates with habit percentages derived from the statistics of a number of field campaigns. The detailed information regarding the information on particle habits and size distributions used in MOD06 can be found in King

et al. (2003). The relationships between the particle size definitions used in this paper are discussed in Appendix B. We find in this case that the effective sizes agree well between the MOD06 and Z-Velocity algorithms with the mean values near 30 μm and 28 μm, respectively. The standard deviation of the MOD06 sizes is larger than derived from the ground although this is expected given the wider geographical domain evaluated compared to the effective domain examined by the ground-based data. The MOD06 IWP also has a wider spectrum ranging from 5 gm^{-2} to 120 gm^{-2} and a lower modal IWP of about 53 gm^{-2}, while the ground-based retrieval has a narrower spectrum ranging from 30 gm^{-2} to 90 gm^{-2} and a bi-modal frequency distribution with one mode similar to the MOD06 result and the other somewhat higher at about 62 gm^{-2}. Both satellite and surface retrieved optical thickness vary from 1 to about 5, while the mode value from MOD06 is 2.5 and that from surface measurement is around 3.4. However, the mean optical thickness for both methods is similar at around 2.4 with a standard deviation of 0.34 and 0.68 for the ground-based and MOD06 results, respectively.

Figure 3 also shows a comparison of cloud optical properties retrieved using MODIS data by the Clouds and the Earth's Radiant Energy System (CERES) science team (Minnis et al. 1995, 1998, 2002). These pixel-level retrievals are used internally by the CERES team, though statistics averaged over the CERES sensor footprints are archived along with other CERES data. The default cloud particle effective radius is derived from the 3.7 μm MODIS band (as opposed to default use of the 2.1 μm band by MOD06). The MODIS-CERES particle size tends be larger on average (~32 μm) and spread over a wider range compared to the ground-based retrievals. The comparisons for this case are summarized in Table 1.

Since certain assumptions have been made in the formulation of the ground-based retrieval algorithm, there is some inherent error in the statistics derived from the retrieval results. Using a realistic comparison to aircraft in situ data, the algorithm uncertainty is found to be on the order of 60% in IWC and 40% in mean particle size (Mace et al. 2002). However, the precision of the results seems to vary substantially from case to case due primarily to the ability of the processing methodology to accurately separate air motions from the particle motions in the Doppler velocity. This error introduces a difficult to quantify case-dependent bias in the results. Other algorithm assumptions also contribute

to the error. For instance, we assume that the cirrus particle size spectrum can be approximated by a simple unimodal exponential function. While bimodal size distributions are a frequent occurrence at warmer than average cirrus temperatures and at larger than average radar reflectivities for cirrus, Mace et al. (2002) found using aircraft data that significant error is first encountered at radar reflectivites of greater than about -5 dBZe. Radar reflectivities of this magnitude and greater are found in the middle of the cirrus layer beginning from 17:15:00 UTC (Figure 3a) and contribute to the IWP mode found near 60 gm^{-2}. However, the comparisons suggest that the three retrieval algorithms interpreted the cloud field on this day in a reasonably similar manner. Curiously, however, we do find substantial biases between the MOD06 retrievals of cloud top pressure and temperature compared to the ground-based observations (Figure 4). This cloud-top bias is discussed further in the following section.

3. Comparison of thin cirrus

While the Z-Velocity algorithm shows considerable promise as a tool for cloud property validation, this algorithm is still undergoing development and testing and has not yet been extensively applied to the ARM data. Therefore, for a more general comparison of retrieved cirrus properties we use the Z-Radiance algorithm (Mace et al. 1998). A description of the updated algorithm, a sensitivity analysis, and in situ validation are given in Appendix A. Identifying cirrus based on a temperature and radar reflectivity based definition described in Mace et al. (2001), we show that the IWP and the layer-mean effective radius can be derived to within 20% compared to in situ data.

Traditionally, the approach to validation is to gather events that lend themselves to comparison of one result against another. When enough events have been compiled to form a statistically significant set of comparisons, some estimate of the goodness or lack thereof can be ascertained. While this approach is reasonable, it can take considerable time to gather a set of narrowly defined cloud events that occured when all the necessary ground-based instruments were operating and the satellite passed overhead and successfully observed the cloud field. We have found many circumstances where the MOD06 algorithm does not attempt retrievals in situations that appear obviously cloudy from the ground-based perspective. Consider the data collected on 22 March 2001.

Figure 5 shows the MMCR data collected during the overpass period while the cloud properties retrieved from the Z-Radiance algorithm are shown in Figure 6. Figure 7 shows the 1.38 μm channel MODIS imagery and the associated MOD06 retrieved optical thickness. In this case, the viewing zenith angle is 2.5°. The thin cirrus is overcast during the 3 hours around the overpass time according to the MMCR; however, it thins considerably in the time series during the period after the overpass. When we track along the wind direction (285°) with a speed of 30m/s, there are only 801 points from the 2770 MODIS pixels that have identified cirrus occurrence. The time series of ground-based retrievals suggests that the cirrus becomes quite thin with optical thickness less than 0.5 during the period after the overpass. From the frequency distribution of the MOD06 optical thickness displayed in Figure 8, the modal optical thickness is around 1 while few, if any, MOD06 retrievals of optical thickness are found less than 0.5. The derived cloud-top pressure (Figure 9) is also much higher for this event than the radar-observed cloud top pressure.

a. Comparison of individual cases

Table 2 lists 15 Terra overpasses of the SGP ARM site from 2000 and 2001 that have cirrus of the proper type (optically thin and single layer) existing concurrently with all necessary ground-based data. Our criteria for choosing cases also required that middle level and lower clouds not be present within the along-stream rectangle diagnosed from the wind profiler observations. Thus, after applying all these requirements only 15 candidate cases were available for comparison. No other screening criteria were imposed. Generally, at least several hundred MODIS pixels were available within the rectangular region. Figure 10 shows the comparison of the Z-Radiance and MOD06 cirrus properties. In these comparisons, the satellite-derived mean and standard deviation are compiled using the technique outlined in the previous section while 1 hour of Z-Radiance data are used to form the mean value shown in the plot. The error bars attributed to the ground-based results are the fractional uncertainties that we derived from the aircraft data comparison shown in Appendix A. There are 9 cases of the 15 for which the pixel-level MODIS-CERES retrieval results are available (Figure 11). A summary of the

comparison is in Table 3 where we show the linear correlation coefficient, the slope of a best fit linear regression, the bias, and the bias standard deviation.

Clearly, we have an insufficient number of events to form a statistically meaningful comparison, although useful information-if not generalities-can be inferred from them. One must, therefore, take care in interpreting the statistics in Table 3. We do find some degree of linear correspondence in all the comparisons. The bias in the MOD06-derived IWP, r_e, and optical thickness are slightly positive. The comparison between the ground-based results and the MODIS-CERES retrievals do not show an obvious bias at small optical depths. This leads to an overall better statistical comparison with the caveat that fewer cases were available from MODIS-CERES.

The disagreement between the satellite and ground-based cloud properties may arise from several sources of uncertainty associated with the satellite and ground-based retrieval algorithms. As an example, horizontal and vertical inhomogeneity certainly contributes to the differences in the results. For midlatitude cirrus clouds, it has been observed that ice crystals in the top layers are normally small pristine particles with well-defined hexagonal structures, whereas ice crystals near cloud base tend to be larger irregular particles (Heymsfield et al. 2002). The effect of this inhomogeneity is small for visible channels, but it can be quite significant for shortwave infrared and infrared channels for which ice is strongly absorptive. Another source of error arises from the complexities of the angular scattering of shortwave radiation in cirrus. In order to compile the 15 cases included here, we used view zenith angles that range from very small to very large and covered a range of solar zenith angles. Ideally, we would like to characterize the errors as a function of relative zenith, but this will require additional time to build up the case study data set. Also, since we are concerned primarily with optically thin clouds, any error in the assumed surface albedo will increase error in the satellite-derived results. For example, a cirrus cloud with an optical thickness of 0.5 over a black surface might be expected to have a bidirectional reflectance in the range 3-4% for a visible band and typical solar/viewing geometries. Spectral surface albedo maps used by MOD06 (Platnick et al. 2003) for the MODIS 0.65 μm band vary from about 8-13% for crop mosaic and grassland ecosystems of the SGP region, a range as large as the cirrus reflectance itself.

However, even though the number of cases is small, making the comparison preliminary, intriguing aspects can still be deciphered from the them. For instance, it appears that there is a tendency for the error bias in the spatially averaged MOD06 results to increase for increasingly thin cirrus fields, while this tendency is not seen in the MODIS-CERES results. This behavior may be due to the fact that the cloud identification scheme in the MOD06 product is being applied conservatively over this ecosystem because of the impact of the aforementioned surface albedo uncertainty on both cloud masking and the retrievals, and so some cloudy pixels are not being processed. This would tend to cause the area-averaged cloud properties to be biased high and would tend to cause the bias to increase as the cloud fields in question become more optically thin on average. However, it should be noted that processing these thinner cirrus scenes would have necessarily added significant retrieval uncertainty, as well as a bias if the surface spectral albedos were not specified to an accuracy much greater than the cirrus cloud reflectance.

In order to examine the validity of the cloud top retrievals, the cloud top heights are compared between the surface data and the satellite data. We convert the cloud top pressure and temperature found in the MOD06 files to cloud top height using thermodynamic profiles collected at the ARM site. Based on the comparisons in Figure 12 and Table 3, we find that the satellite-derived cloud top heights are generally lower than those detected by the ground-based cloud radar. This bias appears to be more pronounced in the MODIS-CERES retrievals than in the MOD06 results. The MOD06 cloud top product for high clouds is based on the CO2 slicing algorithm. The fundamental retrieved quantity is cloud top pressure with the corresponding temperature being determined from model analysis (Platnick et al. 2003). The algorithm assumes the attenuation of upwelling radiation in the MODIS CO2 bands by a cloud occurs at a single level in the atmosphere (Wylie and Menzel 1999). Therefore, in tenuous cloud layers, or multiple cloud layers, it is the height corresponding to a radiatively equivalent infinitesimally thin cloud that is estimated. While the CO2 bands are known to be more sensitive than infrared window techniques (e.g. Jin et al. 1996), the retrieved pressures are likely to be lower in the atmosphere than more sensitive active retrievals.

b. Statistical comparison

It is a challenge to acquire a statistically significant set of events when cirrus, satellite, and ground-based instrumentation all exist at a particular location simultaneously. Because of this, we would like to explore an approach which allows us to examine the similarity of certain relationships within the ground-based and satellite-derived descriptions of cirrus. We assume that in the region surrounding the ARM site the properties of a given class of cirrus are similar to the same class of cirrus observed at the ground site. In essence, this assumption allows us to compile statistical distributions of some quantity from clouds observed at the ground site during periods when clouds are present but MODIS is not and compare these distributions to similar distributions compiled from MODIS retrievals of cirrus that do not necessarily occur at the ground site but within the region surrounding it. We have collected the overpasses of 648 events (168 of them that have cirrus clouds) from March 2000 to July 2001 when Terra passed near the SGP site in the daytime and identify cirrus within a 100 km x 100 km area centered on the SGP site. The cirrus reflectance and the cloud top pressure in the MOD06 file are used to identify the occurrence of cirrus. When the cirrus reflectance indicates the presence of cloud, the cloud top pressure of a pixel is less than 500 hPa, and the optical thickness is less than 5, this pixel is counted in the statistics as cirrus. We consider 895,243 MOD06 high cloud retrievals in the 100 x 100 km region during the study period.

We compare the composite properties of MOD06 cirrus observed in the SGP region with similar properties derived from the Z-Radiance algorithm for the same time period in terms of years and months as the MODIS data amounting to a total of 5772 3-minute averages or approximately 300 hours of cirrus. The occurrence distribution of the MODIS pixels and the SGP points categorized by optical thickness are depicted in Table 4. Clearly, the MODIS and ground-based distributions are weighted much differently with respect to optical thickness. For the ground-based data, the thinnest optical thickness bin contains greater than a factor of three more events than the 0.5-1 optical thickness bin with the number of occurrences decreasing exponentially toward higher optical thicknesses. Similar distributions of cirrus optical thickness have been reported in other ground-based mid latitude data sets (Mace et al. 2001; Comstock and Sassen 2003;

Comstock et al. 2002). The MOD06 frequency, on the other hand, peaks in the 1.0-1.5 optical thickness bin with more than an order of magnitude fewer pixels in the 0. -0.5 optical thickness class. This behavior lends some credence to the idea that the bias identified in Figure 12 arises from the MOD06 algorithm not processing thin cirrus pixels over this region.

The frequency distributions of MOD06 and Z-Radiance r_e and IWP within several visible optical thickness ranges are shown and compared in Figures 13-16. It is interesting to note that the effective radius distributions for the various optical thickness ranges do not change a great deal from the thinnest to thickest optical thicknesses considered here. There is a tendency for the mean and mode particle size to increase from the thinnest to thickest optical thickness classes, but the distributions tend to remain broad. The IWP does shift noticeably from a narrow nearly Poisson distribution shape to a somewhat skewed Gaussian distribution for the higher optical thickness classes. Note the skewness changes from the smaller to larger values of IWP as we shift from the 1-3 to the 3-5 optical depth classes. While there are differences in the details, the MOD06 and the Z-Radiance statistics show rather remarkable agreement. The shapes of the distributions and their trends are nearly identical. This agreement suggests that when cirrus are identified in this region, the MOD06 algorithm describes their properties as a function of optical depth in a manner similar to the aircraft-validated Z-Radiance algorithm results. We do note, however, that this statistical comparison only accounts for the properties of cirrus when retrieved by the MOD06 algorithm. The thin cirrus detection bias (explained in section 1a) accounts for the difference in the distribution shapes in the smallest optical depth class. Note that the Z-radiance results suggest a Poisson distribution shape of IWP while the MOD06 IWP mode is shifted slightly to the next highest IWP bin. The smaller particle sizes in this class found by the Z-Radiance algorithm likely arise due to the detection bias. Aside from this, however, the overall agreement suggests that when the cirrus are identified and the retrieval algorithm is applied, the results are in general agreement with the Z-Radiance results that are retrieved with the ground-based data.

4. Summary

In order to improve our understanding of the role clouds play in the climate system, global cloud property retrievals are being conducted using the data sets being created by MODIS on the Terra and Aqua satellites. The retrieval algorithms that are implemented by the MODIS atmospheres team (MOD06; Platnick et al. 2003) and by the CERES science team (MODIS-CERES; Minnis et al. 1995) use visible and shortwave- and/or midwave-infrared reflectances to infer the optical thickness and effective particle size of underlying clouds. While several recent studies have examined the validity of water cloud properties derived from the MODIS sensor (Dong et al. 2003), the error characteristics of these data sets for other cloud types including cirrus are largely unknown. In order for these global cloud products to be utilized for their intended purposes, validation continues to be necessary. Using data collected at the ARM SGP site, we have made a first attempt at using ground-based data to systematically validate cirrus cloud property retrievals from the MODIS algorithms.

The approach we have taken links the ground truth supplied by in situ aircraft data to results obtained by algorithms applied to satellite data as the satellites passed over the ARM site where algorithms applied to ground-based data serve as an intermediate step. This approach requires a thorough validation of the ground-based algorithms with aircraft data and development of an extensive set of satellite-ground-based events. While neither of these requirements has been satisfied to a level where statistical significance can be unambiguously established, we decided to present the data here in a preliminary form to illustrate the general approach and to consider some early generalizations of our findings so that improvements can be pursued while the data sets continue to grow.

Several issues were addressed that make comparison of passive satellite imager retrieval results with ground-based data a challenging exercise. These range from issues associated with establishing the validity of the ground-based retrievals (Appendix A) to accounting for differences in the definitions of effective particle size between the various algorithms (Appendix B). Also, since clouds pass over the narrow field of view and vertically pointing ground-based instruments as they are advected along the wind, some technique beyond simple spatial averaging of a heterogeneous cloud field must be considered in order to conduct reasonable comparisons. This preliminary step in the comparison process is especially important in cirrus clouds since cirrus tend to exist in

fast moving airstreams and have significant heterogeneity across the flow. Using wind profiler-observed horizontal wind direction and speed and knowledge of the cloud location in the vertical column, we were able to construct a rectangular box within the imagery whose long axis was oriented along the wind direction with a length proportional to 1 hour of advection time (30 minutes upstream and 30 minutes downstream of the ground site). This rectangular region was centered on the ground site and had a cross stream length of 30 km. We found that comparisons of the MODIS retrievals averaged over a region defined in this way to 1 hour of ground-based data centered on the overpass time provided superior results compared to simple regional averages that did not consider the advective streamline.

A set of 15 individual events were compiled from Terra MODIS overpasses of the ARM SGP site during 1999 and 2000 when single layer optically thin cirrus were observed by the MMCR. The Z-Radiance algorithm (Appendix A) was applied to this data and the comparisons presented in Figures 10 and 11. We found that a degree of linear correlation exists in the comparisons considered here. Overall, the optical depth shows the best comparison with the ground-based results while the effective radius has more spread in the comparison. The source of disparity in the spatially-averaged MOD06 results occurred preferentially when the optical thickness of the cirrus retrieved from the radar data was less than about 0.5. As discussed, MOD06 takes a more conservative approach to the detection of thin cirrus before a retrieval is attempted. In several cases, the optical thickness derived from the ground-based data decrease to values approaching 0.5, while the area averaged MOD06 optical thickness remain larger. In layers that were more optically thick, both satellite and ground-based algorithms appeared to perform equally well when compared to each other. These findings have clear implications for the spatially averaged Level-3 products being created with MOD06 retrievals (MOD08_D3) and suggest that cirrus cloud properties over continents may be biased toward the less frequent optically thicker cirrus clouds. Though there is an apparent MOD06 bias in the thin cirrus comparisons, what has not been studied is the occurrence of false positives in these satellite algorithms; i.e., cases where retrievals are attempted but cirrus is not detected from the ground or not thick enough to allow for reliable retrievals from solar methods. Overall, satellite biases relative to the ground-based

retrievals derived in the present study are incomplete until such false posititive statistics are known.

Reasoning that the properties of clouds observed in a region surrounding the ARM site by MODIS should be similar to the properties of the clouds observed at the ARM site by the ground-based instruments, we relaxed the requirement that the clouds be observed simultaneously by both instruments and examined the frequency distributions of IWP and r_e for different optical thickness classes. Comparing MODIS-derived high cloud properties in a 10^4 km^2 region centered on the SGP site from 168 cloudy overpasses with cirrus properties derived from ground-based data collected during the same period of time (March 2000-July 2001), we found that the frequency distribution of optical thickness for high clouds in the MOD06 revealed the thin cirrus detection bias (Table 4) with relatively few occurrences of cirrus with optical thickness less than 0.5 as compared to the ground-based data where the optically thinnest clouds were the most frequently observed. Comparing the derived microphysical properties in various optical thickness classes, we found that the frequency distributions of IWP and effective radius agree well. While the details of the comparisons are not in exact agreement and the MOD06 detection bias skews the result to larger IWP and particle sizes in the <0.5 optical thickness class (Figure 13), both algorithms show a similar trend in IWP and particle size for changing optical depth. As the optical depth increases, the modes of the broadly distributed particle size histograms shift toward larger values while the IWP distributions evolve from a Poisonian shape in the low optical depth classes to skewed Gaussian distributions at the higher optical depth range.

This work is preliminary in the sense that many more cases are needed to establish a reasonable degree of statistical significance so that numerical values can be applied to the uncertainties in the retrieved cloud properties. So long as the ground-based instruments operated by the ARM program continue to function, only time is needed to generate additional coincident cases. Our eventual goal is to investigate the error characteristics in the MODIS-derived cloud properties as a function of the viewing geometry of the instrument and as a function of ecosystem. For instance, do we find similar thin cirrus biases over the tropical oceans or over the polar regions? Since we have only examined cases observed by MODIS on the Terra satellite, do we find similar

issues with the MODIS instrument on Aqua? Also, since the MODIS cloud mask algorithm varies with ecosystem type as does the MOD06 assignment of spectral surface albedos, each ecosystem should be considered separately. We expect to find significant sensitivity to errors in the assigned spectral surface albedo, especially for thin cirrus retrievals.

In terms of improving our confidence in the ground-based retrievals, additional aircraft data are clearly needed to establish more rigorous uncertainties in the ground-based algorithm results. Since statistical significance in validation will not be accomplished without an increase in the number of direct aircraft-ground site comparisons, it seems clear that if the atmospheric research community places value on rigorously characterizing the uncertainties in global cloud property retrievals, then an investment in the quantity of aircraft-ground site comparisons should be a high priority.

Acknowledgements. This research would not have been possible without substantial assistance from several individuals on the MODIS Atmospheres and CERES science teams including Dr. William Ridgway who provided access to MODIS data and products. Mr. Michael Poellot and the University of North Dakota Citation team worked hard during several field campaigns at the ARM SGP site. Sally Benson was instrumental in developing visualization tools for the MODIS data. Data were obtained from the Atmospheric Radiation Measurement Program sponsored by the U. S. Department of Energy, Office of Science, Office of Biological and Environmental Research, Environmental Science Division. Specifically, we would like to thank Mr. Jim Teske and staff at the SGP site for keeping the instruments functioning and the data flowing in a sometimes challenging environment. Primary funding for this work was provided by a NASA EOS Validation Program grant (NAG56458), by the Environmental Science Division of the U. S. Department of Energy (Grant DE-FG0398ER62571). P.Y. was supported in this work by NSF grant (ATM-0239605) and NASA grant (NAG-1-02002). The CERES MODIS retrieval results were provided by Sunny Sun-Mack and developed with support by the NASA Earth System Enterprise through the CERES Project. Additional support provided by the U.S. Department of Energy via Interagency Agreement DE-AI02-97ER62341.

Appendix A: The Z-Radiance Algorithm

The Z-Radiance algorithm (Mace et al. 1998; Zhang 2002) retrieves the layer-mean properties of optically thin cirrus by combining radar reflectivity observations from the MMCR and radiances measured by the Atmospheric Emitted Radiance Interferometer (AERI) at the ARM sites. We assume that the layer-mean particle size distribution (PSD) can be approximated by a modified gamma function that can be written,

$$N(D) = N_x \exp(\mathrm{a})\left(\frac{\mathrm{D}}{\mathrm{D_x}}\right)^{\mathrm{a}} \exp\left(-\frac{D\mathrm{a}}{D_x}\right) \qquad \text{(A.1)}$$

(Mace et al. 1998) where D_x is the modal diameter and N_x is the number of particles per unit volume per unit length at the functional maximum.

Assuming that the particles are small compared to the wavelength, we can use the Rayleigh scattering approximation and express the forward model equations as

$$Z = N_x e^{\alpha} D_x^{7} \frac{(6+\alpha)!}{\mathrm{a}^{7+\mathrm{a}}} \qquad \text{(A.2)}$$

$$\varepsilon = 1 - \exp[-(1-\overline{\omega_0})\,\overline{\beta}\Delta h] \qquad \text{(A.3)}$$

In equation A.2, Z is radar reflectivity factor. In equation A.3, e is the beam emittance at some wavelength, $\overline{w}_o$ is the single-scatter albedo, and $\overline{b}$ is the extinction coefficient. In equation A.3, e is the beam emittance at some wavelength. By relating the extinction coefficient and single scattering albedo to the PSD parameters (D_x and N_x) using the radiative parameterization described by Fu et al. (1998) and the definition of the effective radius and IWC calculated by integrating equation A.1.

Through an iterative scheme, a cloud layer mean PSD is found that simultaneously expresses the observed radar reflectivity and the downwelling radiance as observed by the AERI when the radiative properties of the particle distribution are inserted into the MODTRAN3 radiance algorithm (Berk et al. 1989).

To estimate the sensitivity of the Z-Radiance algorithm to uncertainties in the input data, we use a fractional deviation which is defined as

$$\delta^{2\sigma}_{IWC\,r\,e} = \frac{C_{sta} - C_{dev}}{C_{sta}} \tag{A.4}$$

where C_{sta} is the IWC or r_e value calculated using an unperturbed radar reflectivity factor and an unperturbed layer emittance, C_{dev} is the IWC or r_e value calculated using a perturbed radar reflectivity or a perturbed layer emittance.

In the sensitivity analysis of the Z-Radiance algorithm, a representative range in radar reflectivity from –6 to –40 dBZe is used and the cirrus emittance is varied from 0.1 to 0.9. The layer thickness is set to 1 km. Because the calibration error for the MMCR is about 1 dBZ, the deviation from the representative values is assumed to be multiples of 1 dBZ. And because the AERI radiance error is relatively small, we use multiples of 0.01 (less than about 10% of representative values for cirrus emittance) as the deviation. Shown in Figure A.1 and Figure A.2, we find that calibration errors up to 5 dBZ in the radar lead to errors as large as 50% in the IWC and 22% in the effective radius with an inversely proportional relationship between the calibration errors and the retrieved values. Errors in the AERI radiance up to 5% result in IWC errors of 13% and errors in the effective radius of just -4%.

Since in situ measurements can provide reliable information about actual cloud properties, microphysical data collected in cirrus clouds by aircraft are also used to establish the validity of the Z-Radiance algorithm. The University of North Dakota (UND) Cessna Citation II aircraft, has been used in research projects for the ARM Program during intensive observing periods (IOPs) between 1997 and 2000 (Poellot et al. 1999) with Particle Measuring Systems (PMS) probes (Knollenberg 1970).

The basic measurement consists of the maximum dimension of ice particles observed over a 5-second period. The observations are then reduced into a distribution of the number of particles observed within certain size ranges. From this we calculate the ice water content and effective radius. It has been shown that the bulk density of cirrus particles decreases with an increase of their dimension D (Brown and Francis 1995). This characteristic of cirrus results in substantial difficulty when attempting to derive water content from measured particle spectra. There have been many schemes for

parameterizing the masses (M) of ice particles to determine the ice water content. In this study, the M-D power laws proposed by Mitchell (1996) are used:

$$M = \alpha D^{\beta} \tag{A.5}$$

The coefficients are listed in Table A.1. These particle habits correspond to the typical range of particle habits observed in midlatitude cirrus clouds. The masses of ice crystals vary substantially when calculated with different coefficients. Therefore, for every size distribution, we calculate the ice crystal mass for every kind of crystal shape listed in Table A.1 and then consider the mean and standard deviation of the various habits to allow for a reasonably estimated range of uncertainty of the IWC sampled by the aircraft.

The clouds were sampled by the UND Citation with a flight strategy that was designed to generate an unbiased statistical sample of the cirrus layer properties as they advected over the ground-based instrument suite. The aircraft started either near cloud base or top and stepped up or down at approximately 300 m increments after performing a level leg of approximately 20 km centered on the SGP ground site. The cloud layer was profiled in this way and then a spiral of approximately 5 km radius was conducted centered on the SGP site through the layer. This pattern was repeated as long as the cloud and aircraft fuel permitted.

Depending on the flight profile (level legs or spiral) we use two approaches to calculate the ice water path from in situ measurements: first, for a series of stepped level legs that profile the cloud layer, the leg-averaged value of IWC are considered valid over a vertical depth that is taken to equal the aircraft altitude change between legs. The vertical integral is approximated as the sum of these legs. For the spiral profile, a more robust integral is approximated by summing the IWC over the vertical depth applicable to each 5-second interval.

A comparison of 13 individual cases between the layer-mean retrieved cloud properties and similar properties derived from aircraft profiles of cirrus using data collected during cloud IOPs at the SGP site is shown in Figure A.4. Because the 2DC is most reliable in the particle range between approximately 100 and 700 microns, we compare the IWC and effective radius only in that size range; the observed and retrieved size distributions are integrated from 100 μm to 700 μm. As can be seen in Figure A3, we find a high degree of linear correspondence between the observations and the retrievals.

The linear correlation coefficient is 0.92 for IWP comparison and 0.91 for the r_e comparison with an RMS for both r_e and IWP between 20% and 25% of the mean values.

To build further confidence in the retrieval results, the solar radiative effects derived from layer-averaged cirrus properties are also examined. Since the cirrus-layer properties derived from the retrieval algorithm will produce the correct downwelling radiation in the infrared portion of the spectrum, we compare, when possible, the downwelling solar flux observed at the surface with calculations of the solar flux that use the derived microphysical properties.

The observed fluxes are expressed in terms of the fraction of the clear sky flux at the surface removed by the cloud layer, that is, the solar forcing which is employed in many radiative field studies (Shi 1994; Mace et al. 1998; Mace et al. 2001). The observed clear-sky fluxes are determined following Long (1996).

The normalized cloud forcing (C_f) is defined as

$$C_f = (F_{clear} - F_{cloud}) / F_{clear} \qquad \text{(A.6)}$$

where F_{cloud} is the observed downward surface shortwave flux in the presence of clouds, and F_{clear} is the clear-sky value calculated from the radiative parameterization.

The solar forcing calculated from the retrieved cloud properties from July 2000 to July 2001 at the ARM SGP site is used here. The mean of the calculated forcing values is binned in 0.015 forcing increments, and the standard deviation is calculated. The comparison is shown in Figure A4 which shows the results from a previous version of the algorithm and the present implementation which uses the Fu (1998) radiative parameterization. The correlation coefficient improves slightly from 0.834 to 0.886. The improvement in the updated results can be seen most directly in the 0.15 to 0.35 values of cloud forcing where the linear relation is stronger for the updated algorithm. For small values of cloud forcing (<0.12), the bias is likely caused by limitations of the radar measurements. When cirrus clouds are thin, the radar cannot detect the full depth of the cloud layer, so the layer mean Z_e is likely biased high and the resultant calculated forcing values are biased high also as in Figure A4 for C_f smaller than 0.1. The Z-Radiance algorithm is not applicable to thick cirrus (e = 0.9), so the cloud forcing comparison is limited to values smaller than 0.4. This equates to visible optical thicknesses of around 4.

Appendix B. Cirrus cloud particle size comparison

There have been several studies that have attempted to make sense of the myriad definitions of cirrus cloud particle size (e.g. Mitchell 2002; McFarquhar and Heymsfield 1998). It is important to understand the difference between the definitions of particle size that are used in this paper. Since the electromagnetic frequencies used to probe cirrus range from visible light to microwaves, the observations themselves are naturally weighted to different moments of the particle size spectrum. The retrieval algorithms, evaluated in this paper, are essentially designed to convert from the moments of the distribution measured by the instruments to other moments of interest. Our goal with this paper is to evaluate the relative success of these conversions through comparison. However, we must first understand the definitions of the different particle size descriptions used in the algorithms and the relationships between them.

Since aircraft make the most direct measure of the particle size distribution, the maximum dimension or some variant of it (Brown and Francis 1995) is typically used to describe the sizes of the particles. Use of the maximum dimension as the characteristic ice particle dimension has resulted in a number of authors attempting to quantify the amount of condensed water and projected ice surface area within the volume of a sphere or circle circumscribed around the maximum dimension (e. g. Heymsfield and Platt 1984; Mitchell 1996; Heymsfield et al. 2002). Such papers often discuss an effective ice crystal density ($?_{eff}$) that decreases from that of solid ice for small spheroidal particles to values that are quite low (~0.1 g/cm^3) for millimeter size ice particles (Brown and Francis 1995). These relationships tend to be strongly habit dependent as shown by Heymsfield et al. (2002) and others. In order to facilitate comparison between aircraft data and cloud properties retrieved from ground-based radar data, we have derived the ground-based retrieval algorithms in terms of particles sizes related directly to the maximum dimension. This decision has necessitated that we specify some relationship between the size and effective density where we use the definition reported by Brown and Francis (1995) in the Z-Radiance algorithm and by Mitchell (1996) in the Z-Velocity algorithm.

Retrieval algorithms that use optical measurements typically retrieve the effective radius (r_e) which is defined by Hansen and Travis (1974) for spherical particles as the ratio of the third moment of the size distribution to the second moment of the size distribution or

$$r_e = \frac{\int a^3 n(a)\, da}{\int a^2 n(a)\, da} = \frac{\langle a^3 \rangle}{\langle a^2 \rangle} \tag{B.1}$$

where a is particle radius and the angle brackets denote an integration over the size spectrum to derive a moment. It can be shown easily that in the case of particles that are large with respect to the wavelength of light (i.e., the case when extinction efficiency is approximately 2), the effective radius is related in a simple manner to the optical thickness and the ice water path, $r_e = \frac{3}{2}\frac{w}{t}$ where w is the ice water path, t is the optical thickness, and ? is the density of water. In the case of spherical particles, the effective radius that is calculated with this relationship has a direct physical connection to the size distribution. In the case of nonspherical particles, the interpretation is more complicated. For the satellite algorithms, the retrieved effective radius can be expressed as $r_e = \frac{3}{4}\frac{V}{A_{pro}}$ and interpreted as the ratio of the volume of ice V (or by way of the solid ice density to the condensed mass) to the cross sectional area (A_{pro}). This cross sectional area is a habit-dependent parameter that complicates the interpretation of the effective radius as a simple ratio of distribution moments. For MOD06, we assume a mixture of habits whose fractional abundances depend on particle size (King et al. 2003). For a particular habit, A_{pro} is given by the empirical dimensional power laws reported in Mitchell (1996); i.e. $A_{pro} = a_A D^{b_A}$ where D is maximum dimension. The MODIS-CERES particle sizes are based entirely on varying distributions of solid hexagonal ice columns of varying lengths (L) and widths (D). The effective radius reported here is the effective diameter D_e (Minnis et al. 1998) divided by 2. The value of D_e is the same as that defined by Ou et al. (1993): $D_e = \int D^2 Ln(L)\, dL / \int DLn(L)\, dL$. A constant density of 0.9 g cm^{-3} is used for all crystals in both the MOD06 and the MODIS-CERES algorithms.

The complicating factors in comparing the particle sizes arise from the effective density relationship used in the Z-Radiance algorithm and the projected area relationships used in the MOD06 retrieval. If we assume that the water paths retrieved by the two algorithms are equal, it is easy to show that

$$r_{e,MODIS} = p\,\frac{\left\langle a_s^2 \right\rangle r_{egnd}}{A_{pro}} \tag{B.2}$$

where $\left\langle a_s^2 \right\rangle$ represents the second moment of the solid-equivalent modified gamma size distribution (denoted by the subscript *s*);

$$N\left(D_s\right) = N_x \exp(a_s)\left(\frac{D_s}{D_{x,s}}\right)^{a_s} \exp\left[\frac{a_s D_s}{D_{x,s}}\right] \tag{B.3}$$

It is our goal here to derive an expression for $\left\langle a_s^2 \right\rangle$ so that a conversion factor between the sizes can be expressed.

With the Brown and Francis approximation of bulk density and an assumption that the order of the retrieved modified gamma size distribution (a – note the lack of subscript *s*) is unity, the Z-Radiance algorithm estimates N_x and D_x from the radar reflectivity and downwelling thermal infrared radiance (See Appendix A). To convert to a solid-equivalent size distribution, we assume that the total number of particles, N_T, and the ice water content, *iwc*, are the same between the solid equivalent and retrieved size distributions. We assume that N_x is the same also, requiring us to calculate a_s and $D_{x,s}$ to express our size conversion factor. With $r_{eff} = a_r D^{b_r}$, we can integrate the solid and retrieved size distributions to derive the *iwc* and equate the two resulting expressions to arrive at

$$r_{ice} e^{a_s} D_{x,s}^4 \frac{\Gamma\left(4+a_s\right)}{a_s^{4+a_s}} = e^1 a_r C D_x^{4+b_r} \Gamma\left(5+b_r\right) \tag{B.4}$$

In equation (B.4), the left hand side of the equation results from an assumption of solid particles with $?_{ice}$=0.92 g cm^{-3} while the right hand side assumes an effective density relationship adapted from figure 3 of Brown and Francis (1995) where $a_r = 121.6$ and $b_r = -1.08$ (cgs units). The effective density power law relationship is strictly applicable only for particles with a maximum dimension larger than 100 µm although equation (B.4)

is derived by integrating over all sizes. A size-dependent correction factor (C) is derived to account for this. In equation (B.4), a common factor, $\frac{N_x p}{6}$, has been cancelled from the right and left sides. Using similar assumptions, we can equate the total particle concentration of the solid equivalent and retrieved distributions,

$$\frac{D_{x,s} e^{a_s} \Gamma(a_s + 1)}{a_s^{a_s+1}} = D_x e^1 \tag{B.5}$$

where a common factor N_x has been cancelled from both sides. Solving, equation (B.5) for $D_{x,s}$ and substituting into equation (B.4), a_s is derived using a straightforward minimization technique, and $D_{x,s}$ is then easily determined.

With an approximate description of the solid-equivalent size spectrum, we are in a position to calculate

$$\left\langle a_s^2 \right\rangle = \frac{N_x e^{a_s}}{8 D_{x,s}} \int D^{2+a_s} \exp\left(\frac{-D a_s}{D_{x,s}} \right) dD \tag{B.6}$$

where $2a = D$ is used to convert variables in the integration. Finally, A_{pro} is calculated with the fractional abundances of the various habits as follows,

$$A_{pro} = \frac{N_x e^1}{D_x^a} \sum_i^{habits} a_{A,i} f_i \int D^{b_{A,i}+1} \exp\left(\frac{-D}{D_x} \right) dD . \tag{B.7}$$

In equation (B.7), the integration is conducted using the retrieved size spectrum (i.e. N_x, $D_{x,}$, a=1) because the Mitchell (1996) area-dimensional relations are defined in terms of the particle maximum dimension. Following King et al. (2003), $a_{A,i}$, $b_{A,i,}$ and f_i correspond to the various habits. For particles less than 70 μm, f_i has values of 0.5 for bullet rosettes, 0.25 for hexagonal columns, and 0.25 for plates. When D>70 μm, f_i is 0.3 for aggregates, 0.3 for bullet rosettes, 0.2 for columns and 0.2 for plates.

Using the conversion factor $p \frac{\left\langle a_s^2 \right\rangle}{A_{pro}}$, Figure B1 shows the ratio of $r_{e,MOD06}$ to $r_{e,gnd}$ plotted as a function of $r_{e,gnd}$. We find, as expected, that $r_{e,MOD06}$ is always smaller than r_e retrieved using the Z-Radiance algorithm assuming an ice effective density lower than solid ice and that the effect is largest at the smallest particle sizes. Given that the effective density is smallest at the largest particle sizes, one might expect that the

disparity between the MOD06 definition of effective radius and the ground-based retrieval would be largest at the largest sizes. However, the cross sectional area assumed by MOD06 increases less rapidly compared to a spherical particle and there is a tradeoff between the slower increase of cross sectional area to the more rapid increase of $\left\langle a_s^2 \right\rangle$ for a given size. While the conversion function is monotonic, its rate of change varies with size in the 30-50 μm range due to the different particle habit weighting of the MOD06 A_{pro}.

References:

Ackerman, T. P., K. N. Liou, F. P. J. Valero, and L. Pfister, 1988: Heating rates in tropical anvils. *J. Atmos. Sci.*, **45**, 1606-1623.

Brown, P. R. A., and P. N. Francis, 1995: Improved measurements of the ice water content in cirrus using a total water probe. *J. Atmos. Oceanic Technol.*, **11**, 410-414.

Comstock, J. M., T. P. Ackerman, and G. G. Mace, 2002: Ground-based lidar and radar remote sensing of tropical cirrus clouds at Nauru Island: Cloud statistics and radiative impacts. *J. Geophys. Res.*, **107** (D23), 4714, doi:10.1029/2002JD002203.

Dong, X., and G. G. Mace, 2003: Profiles of low-level stratus cloud microphysics deduced from ground-based measurements. *J. Atmos. Oceanic. Technol.*, **20**, 42-53.

Fu, Q., P. Yang and W. B. Sun, 1998: An accurate parameterization of the infrared radiative properties of cirrus clouds for climate models. *J. Climate*, **11**, 2223-2237.

Heymsfield, A. J., and C. M. R. Platt, 1984: A parameterization of the particle size spectrum of ice clouds in terms of the ambient temperature and the ice water content. *J. Atmos. Sci.*, **41**, 846-855.

Heymsfiled, A. J., S. Lewis, A. Bansemeter, J. Iaquinta, L. Miloshevich, M. Kajikawa, C. Twohy, M. R. Poellot, 2002: A general approach for deriving the properties of cirrus and stratiform ice cloud particles. *J. Atmos. Sci.*, 59, 3-29.

Jin, Y., W. B. Rossow, and D. P. Wylie, 1996: Comparison of the climatologies of high level clouds from HIRS and ISCCP. J. Climate, 9, 2850-2879.

King, M. D., and D. D. Herring, 2000: Monitoring Earth's vital signs. *Sci. Amer.*, **282**, 72-77.

King, M. D., Y. J. Kaufman, W. P. Menzel and D. Tanré, 1992: Remote sensing of cloud,

aerosol, and water vapor properties from the Moderate Resolution Imaging Spectrometer (MODIS). *IEEE Trans. Geosci. Remote Sens.*, **30**, 2-27.

King, M. D., Si-Chee Tsay, S. E. Platnick, Menghua Wang, and K. N. Liou, 1997: Cloud retrieval algorithms for MODIS: optical thickness, effective particle radius, and thermodynamic phase.

King, M. D., W. P. Menzel, Y. J. Kaufman, D. Tanr B. C. Gao, S. Platnick, S. A. Ackerman, L. A. Remer, R. Pincus, and P. A. Hubanks, 2003: Cloud and Aerosol Properties, Precipitable Water, and Profiles of Temperature and Humidity from MODIS. IEEE Trans. Geosci. Remote Sens., 41, 442-458.

King, M. D., S. Platnick, P. Yang, G. T. Arnold, M. A. Gray, J. C.Riédi, S. A. Ackerman, and K. N. Liou, 2003: Remote sensing of liquid water and ice cloud optical thickness, and effective radius in the arctic: Application of air-borne multispectral MAS data. *J. Atmos. Sc.*. (submitted)

Knollenberg, R. G., 1970: The optical array: An alternative to scattering or extinction for airborne particle size determination. J. Appl. Meteor., 9, 86-103.

Liou, K. N., 1986: Influence of cirrus clouds on weather and climate processes: A global perspective. *Mon. Wea, Rev.*, **114**, 1167-1199.

Lynch, D. K., K. Sassen, D. O'C. Starr, and G. Stephens (Eds.). Cirrus (Oxford Univ. Press, New York, 2002).

McFarquhar, G. and A. J. Heymsfield, 1998: The definition and significance of an effective radius for ice clouds. J. Atmos. Sci., 55, 2039-2052.

Mace, G. G., T. A. Ackerman, P. Minnis, and D. F. Young, 1998: Cirrus layer microphysical properties derived from surface-based millimeter radar and infrared interferometer data. *J. Geophys. Res.*, **103**, 23027-23216.

Mace, G. G., E. E. Clothiaux, and T. A. Ackerman, 2001: The composite characteristics of cirrus clouds: Bulk properties revealed by one year of continuous cloud radar data. *J. Climate*, **14**, 2185-2203.

Mace, G. G., A. J. Heymsfield, and Michael R. Poellot, 2002: On retrieving the microphysical properties of cirrus clouds using the moments of the millimeter-wavelength Doppler spectrum. *J. Geophys. Res.*, **107**, 4815-4841.

Mace, G. G., 2003: On retrieving the microphysical properties of cirrus clouds using the moments of the millimeter-wavelength doppler spectrum: Part II An analytical framework and formal error analysis. *J. Geophys. Res.*, in press.

Minnis, P., D. P. Garber, D. F. Young, R. F. Arduini, and Y. Takano, 1998: Parameterization of reflectance and effective emittance for satellite remote sensing of cloud properties. *J. Atmos. Sci.*, **55**, 3313-3339.

Minnis, P., D. P. Kratz, J. A. Coakley, Jr., M. D. King, D. Garber, P. Heck, S. Mayor, D. F. Young, and R. Arduini, 1995: Cloud Optical Property Retrieval (Subsystem 4.3). "Clouds and the Earth's RadAnalyses and Radiance Inversions (Subsystem 4)", NASA RP 1376 Vol. 3, edited by CERES Science Team, pp. 135-176.

Minnis, P., D. F. Young, B. A. Weilicki, S. Sun-Mack, Q. Z. Trepte, Y. Chen, P. W. Heck, and X. Dong, 2002: A global cloud database from VIRS and MODIS for CERES. *Proc. SPIE 3rd Intl. Asia-Pacific Environ. Remote Sensing Symp. 2002: Remote Sens. of Atmos, Ocean, Environ.t, and Space*, Hangzhou, China, (At

HYPERLINK
"http://wwwpm.larc.nasa.gov/ceres/pub/conference/Minnis.SPIE.02.pdf"
http://wwwpm.larc.nasa.gov/ceres/pub/conference/Minnis.SPIE.02.pdf)

Mitchell, D. L., 1996: Use of mass- and area-dimensional power laws for determining precipitation particle terminal velocities. *J. Atmos. Sci.*, **53**, 1710-1723.

Moran, K. P., B. E. Martner, M. J. Post, R. A. Kropfli, D. C. Welsh, and K. B. Widener, 1998: An unattended cloud-profiling radar for use in climate research. *Bull. Amer. Meteor. Soc*, **79**, 443-455.

Ou, S. C., K. N. Liou, Y. Takano, N. X. Rao, Q. Fu, A. J. Heymsfield, L. M. Miloshevich, B. Baum, and S. A. Kinne, 1995: Remote sounding of cirrus optical depths and ice crystals sizes from AVHRR data: Verification using FIRE II IFO measurements. *J. Atmos. Sci.*, 52, 4143-4158

Platnick, S., M. D. King, S. A. Ackerman, W. P. Menzel, B. A. Baum, J. C.Riédi, and R. A. Frey, 2003: The MODIS Cloud Products: Algorithms and Examples from Terra. *IEEE Trans. Geosci. Remote Sens.*, **41**, 459-473.

Poellot, M. R., K. A. Hilburn, W. P. Arnott, and K. Sassen, 1999: In situ observations of cirrus clouds from the 1994 ARM RCS IOP. In *Ninth ARM Science Team Meeting Proceedings*, San Antonio, Texas, March 22-26, 1999.

Rossow, W. B., and R. A. Schiffer, 1999: Advances in understanding clouds from ISCCP. *Bull. Amer. Meter. Soc*., **80**, 2261-2286.

Stephens, G. L., and P. J. Webster, 1981: Clouds and climate: Sensitivity of simple systems. *J. Atmos. Sci.*, **38**, 235-247.

Stephens, G. L., S.-C. Tsay, P. W. Stackhouse, Jr., and P. J. Flatau, 1990: The relevance of the microphysical and radiative properties of cirrus clouds to climate and climatic feedback. *J. Atmos. Sci.*, **47,** 1742–1753.

Webster, P. J., 1994: The role of hydrological processes in ocean-atmosphere interactions. *Rev. Geophys.*, **32**, 427-476.

Wylie, D. P., and W. P. Menzel, 1989: Two years of cloud cover statistics using VAS. *J. Clim.*, **2**, 380-392.

Wylie, D. P., W. P. Menzel, H. M. Woolf, and K. I. Strabala, 1994: Four years of global cirrus cloud statistics using HIRS. *J. Climate*, **7**, 1972-1986.

Wylie, D. P., and W. P. Menzel, 1999: Eight years of high cloud statistics using HIRS. *J. Climate,* **12**, 170-184.

Zhang, Yuying, 2002: On the use of ground-based, aircraft and satellite data for the study of cirrus clouds. *M.S. Thesis*, Univ. of Utah, pp. 133.

Tables

Table 1. Summary of the properties retrieved from data collected on 6 March 2001. Shown are the mean and standard deviation of the properties observed in the rectangular region depicted in Figure 1 for the MOD06 and MODIS-CERES retrievals and in the time series of properties from the ground-based Z-Velocity algorithm shown in Figure 4.

	Z-Velocity	MOD06	MODIS-CERES
r_e (μm)	30.3/1.7	29.9/2.2	31.2/3.1
IWP (g/m^2)	54.0 / 12.7	61.8 / 16.2	59.1 / 18.0
Optical Depth	2.02 / 0.34	2.78 / 0.68	3.08 / 0.83
Cloud Top Temperature (K)	216.2 / 2.2	237.6 / 3.6	
Cloud Top Pressure (hPa)	236.7 / 8.8	359.3 / 28.2	307.7 / 24.5

Table 2. Dates and times of the MODIS data used in the thin cirrus intercomparison. The * denotes Terra cases for which MODIS-CERES cloud analysis has also been performed.

Date (yyyymmdd)	Overpass Time (UTC)	Viewing Angle (°)
*20001127	17:07:14	47.8
*20001128	17:49:55	24.1
*20001130	17:37:39	1.0
*20001220	17:13:04	40.5
20010322	17:35:28	2.1
*20010330	16:46:25	62.9
20010330	18:24:04	62.9
*20010527	17:22:05	21.4
*20010606	17:58:23	42.2
*20010903	17:50:03	34.4
20010904	16:54:58	53.3
20011125	16:40:07	62.7
20011125	18:17:45	63.1
*20011221	17:15:43	22.1
20011228	17:21:45	10.6

Table 3. Statistics of the comparison of thin cirrus properties shown in Figure 12. Shown here are the linear correlation coefficient, the slope of a best fit linear regression line, the mean bias, and the standard deviation of the mean bias compared with the Z-Radiance ground-based retrievals.

	Property	Linear Correlation Coefficient	Slope	Mean Bias	Bias Standard Deviation
MOD06	r_e (μm)	0.424	0.406	1.45	8.16
	IWP (g/m^2)	0.694	1.344	13.13	39.01
	Optical Depth	0.658	1.31	0.67	1.59
	Cloud Top Height (km)	0.809	0.854	-0.586	1.29
MODIS-CERES	r_e (μm)	0.678	0.548	-2.925	6.45
	IWP (g/m^2)	0.763	0.946	-3.345	16.19
	Optical Depth	0.838	1.164	0.210	0.83
	Cloud Top Height (km)	0.592	0.348	-2.482	1.15

Table 4. The number of observations as a function of visible optical depth used in the statistical comparisons shown in Figures 13-16. The percentages shown in parentheses give the frequency of the total number of observations for MOD06 and the ground-based data.

	<0.5	0.5~1.0	1.0~1.5	1.5~2.0	2.0~3.0	3.0~4.0	4.0~5.0
MOD06 pixels	29,259 (7%)	58,150 (14%)	61,976 (15%)	53,145 (13%)	85,774 (20%)	75,785 (18%)	60,348 (14%)
ARM SGP points	3131 (56%)	1003 (18%)	522 (9%)	287 (5%)	331 (6%)	205 (4%)	123 (2%)

Table A.1 Coefficients and exponents to mass-dimensional power laws for various ice crystal types. Random orientation is assumed for D < 100 μm, horizontal orientation otherwise (adapted from Mitchell 1996).

Particle type	α	β	References
Hexagonal plates 100 ~3000 μm	0.00739	2.45	Mitchell and Arnott (1994), Mitchell et al. (1996), Auer and Veal (1970)
Hexagonal columns 100 ~300 μm 300 μm and up	0.00166 0.000907	1.91 1.74	Mitchell and Arnott (1994), Mitchell et al. (1996), Auer and Veal (1970), Heymsfield and Knollenburg (1972)
Crystal with sector-like branches 40~2000 μm	0.00142	2.02	Mitchell and Arnott (1994), Mitchell et al. (1996), Auer and Veal (1970), Pruppacher and Klett (1978)
Broad-branched crystal 100 ~1000 μm	0.000516	1.8	Pruppacher and Klett (1978), Mitchell et al. (1996)
Side plates 300~2500 μm	0.00419	2.3	Mitchell et al. (1990), Mitchell et al. (1996)
Bullet rosettes, 5 branches at 231 K 200~1000 μm	0.00308	2.26	Mitchell (1994), Mitchell et al. (1996)
Aggregates of side planes, columns and bullets 800~4500 μm	0.0028	2.1	Mitchell et al. (1990), Mitchell et al. (1996)

Figure Captions.

Figure 1. (a) Height-Time cross section of radar reflectivity observed by the MMCR at the ARM SGP site on 6 March 2001. Time is shown in UTC hours. (b) Visible image of cirrus observed by MODIS at 1735 UTC in the vicinity of the ARM SGP on 6 March 2001. The SGP central facility is shown with the light green square. The yellow lines show latitude and longitude. The image is created by combining 3 visible channels to create a near true color composite.

Figure 2. Wind profiler data observed by the NOAA 404 MHz wind profiler near Lamont Oklahoma on 6 March 2001. Observations at different times are shown by the symbols.

Figure 3. Comparison of cloud properties retrieved by the Z-Velocity algorithm applied to MMCR data collected at the SGP site and the MOD06 cloud properties retrieved using data collected on 6 March 2001 from within the rectangular region shown in Figure 1. a) shows effective particle radius, b) shows the ice water path and c) shows the optical thickness.

Figure 4. Comparison between cloud top (a) temperature and (b) pressure measured by the MMCR and local radiosonde data and that reported in the MOD06 product.

Figure 5. MMCR height-time cross section of radar reflectivity factor observed on 22 March 2001 at the ARM SGP site.

Figure 6. Layer-averaged cloud properties retrieved by the Z-Radiance algorithm using data collected on 22 March 2001.

Figure 7. (a) MODIS 1.38 micron imagery collected at 1735 UTC on 22 March 2001 over the ARM SGP site and (b) MOD06 optical thickness coincident with the field observed in (a).

Figure 8. Frequency distribution of optical depth from the MOD06 data in the vicinity of the ARM site on 22 March 2001.

Figure 9. Comparison of cloud top temperature and pressure reported in the MOD06 product with observations

Figure 10. Comparison of cirrus properties from the Z-Radiance algorithm and coincident cloud properties reported in the MOD06 product.

Figure 11. Figure 13. As in Figure 12 except the MODIS-CERES data is compared with the Z-Radiance results.

Figure 12. Figure 14. Comparison of cloud top heights reported by (a) the MOD06 product and (b) the MODIS-CERES products with observations at the ARM SGP site.

Figure 13. Figure 15. Comparison of the frequency distributions of effective radius (a) and ice water path (b) for cirrus with optical depths less than 0.5. The MOD06 properties are derived from a 100x100 km region centered on the ARM site for the period beginning in March 2000 and extending to July 2001. The Z-Radiance statistics are derived from cirrus clouds observed during this time period.

Figure 14. As in Figure 15 except for optical depths between 0.5 and 1.0

Figure 15. As in Figure 15 except for optical depths between 1.0 and 3.0

Figure 16. As in Figure 15 except for optical depths between 3.0 and 5.0

Figure A1. Sensitivity of the IWC retrieved by the Z-Radiance algorithm due to error in the input data.

Figure A2. Sensitivity of the effective radius retrieved by the Z-Radiance algorithm due to error in the input data.

Figure A3. Comparison of aircraft-observed IWP and effective radius with retrieved values from the surface instruments. Due to limitations in the 2dc instrument, the observed and retrieved size distributions are integrated only over the 100-700 micron particle size range.

Figure A4. Comparison between calculated and observed downwelling solar fluxes at the surface expressed in terms of the fraction of the downwelling solar flux removed by cloud. (a) solar forcing calculated from Mace98 algorithm, (b) solar forcing calculated from the improved reflectivity-radiance algorithm.

Figure B1. Ratio of the effective radius definition used in the MOD06 algorithm with that used in the Z-Radiance algorithm as a function of the Z-Radiance effective radius.

Table Captions

Table 1. Summary of the properties retrieved from data collected on 6 March 2001. Shown are the mean and standard deviation of the properties observed in the rectangular region depicted in Figure 1 for the MOD06 and MODIS-CERES retrievals and in the time series of properties from the ground-based Z-Velocity algorithm shown in Figure 4.

Table 2. Dates and times of the MODIS data used in the thin cirrus intercomparison. The * denotes Terra cases for which MODIS-CERES cloud analysis has also been performed.

Table 3. Statistics of the comparison of thin cirrus properties shown in Figure 12. Shown here are the linear correlation coefficient, the slope of a best fit linear regression line, the mean bias, and the standard deviation of the mean bias compared with the Z-Radiance ground-based retrievals.

Table 4. The number of observations used as a function of visible optical depth used in the statistical comparisons shown in Figures 13-16.

Table A.1 Coefficients and exponents to mass-dimensional power laws for various ice crystal types. Random orientation is assumed for $D < 100$ μm, horizontal orientation otherwise (adapted from Mitchell 1996).

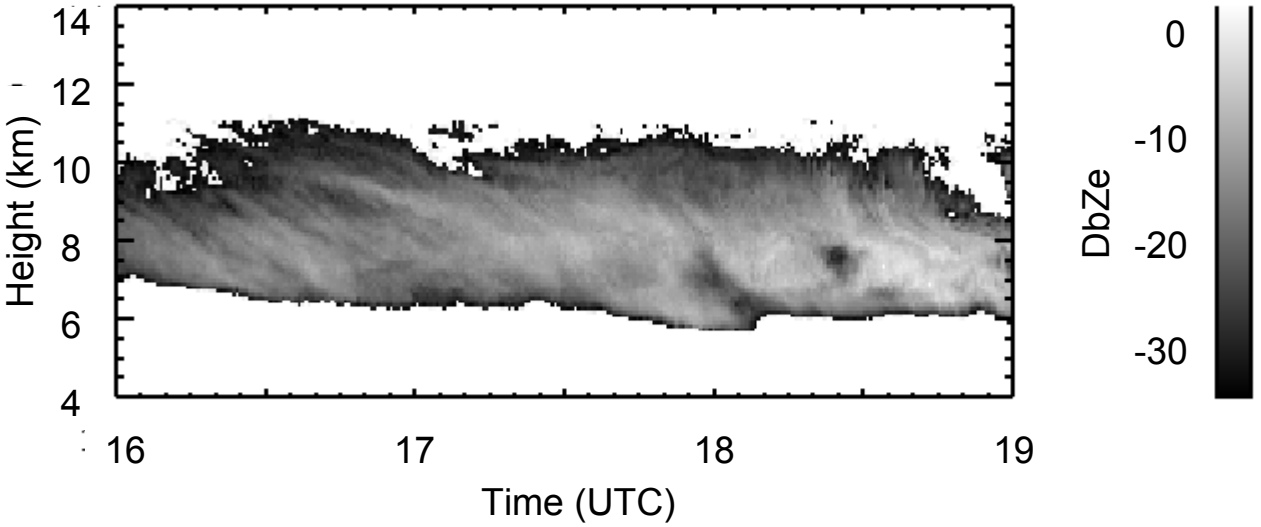

Figure 1a. Height-Time cross section of radar reflectivity observed by the MMCR at the ARM SGP site on 6 March 2001. Time is shown in UTC hours.

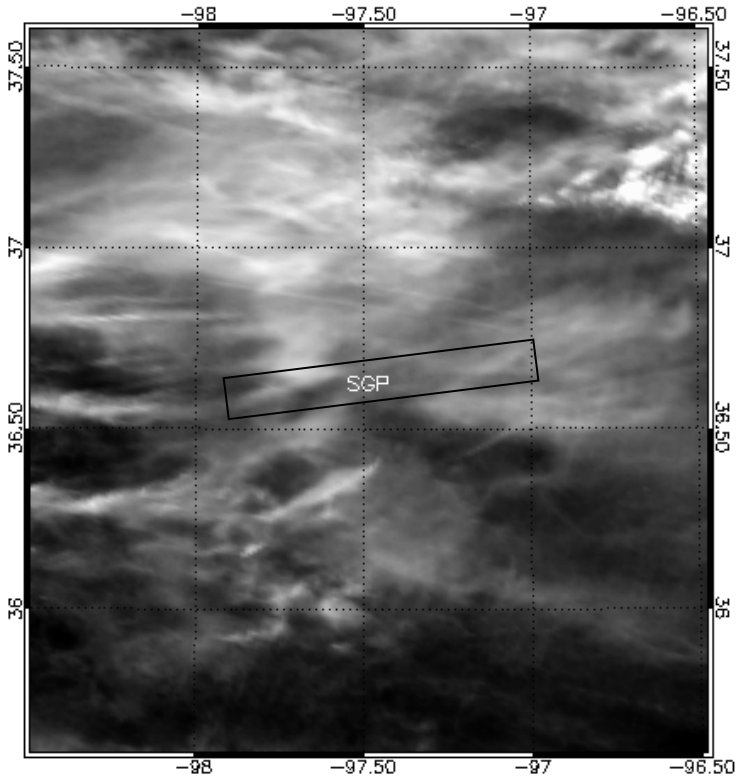

Figure 1b. Visible image of cirrus observed by MODIS at 1735 UTC in the vicinity of the ARM SGP on 6 March 2001. The SGP central facility is shown with the light green square. The yellow lines show latitude and longitude. The image is created by combining 3 visible channels to create a near true color composite.

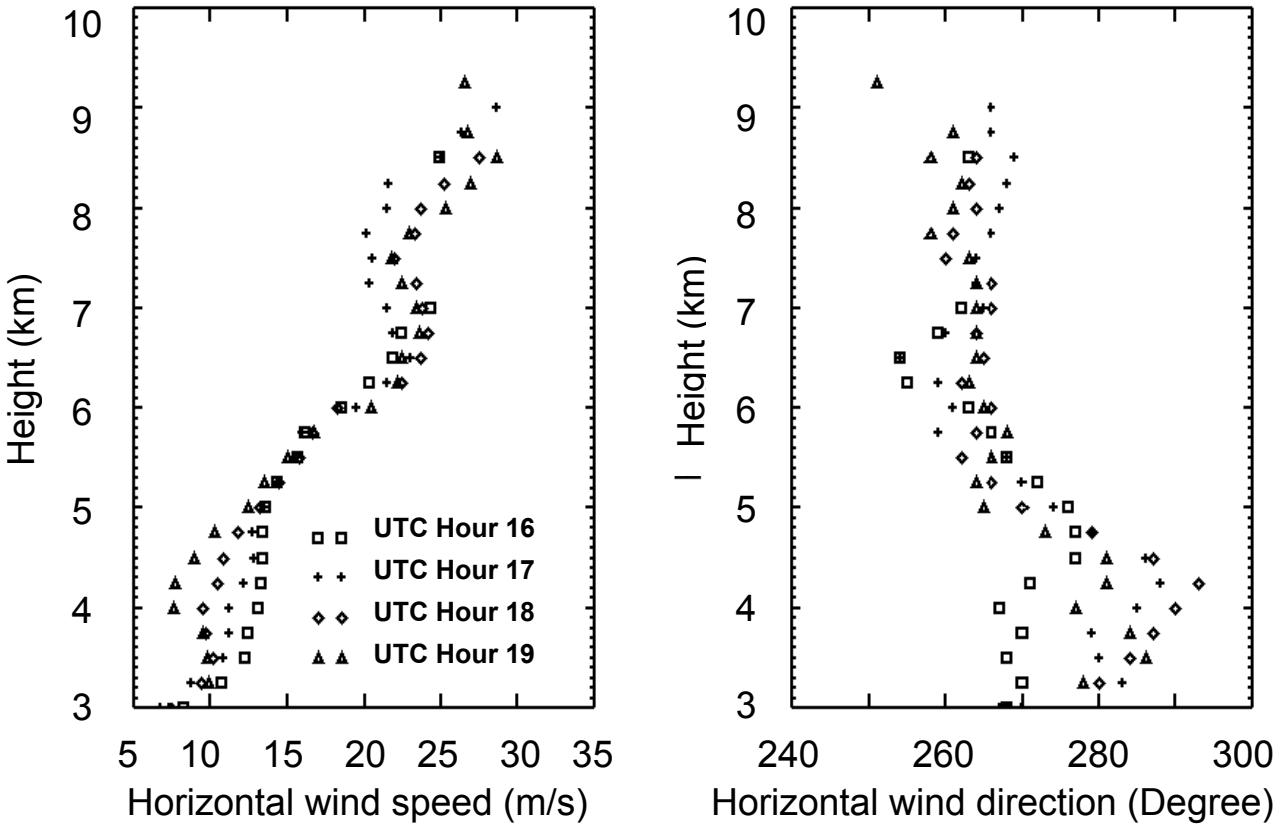

Figure 2. Wind profiler data observed by the NOAA 404 MHz wind profiler near Lamont Oklahoma on 6 March 2001. Observations at different times are shown by the symbols.

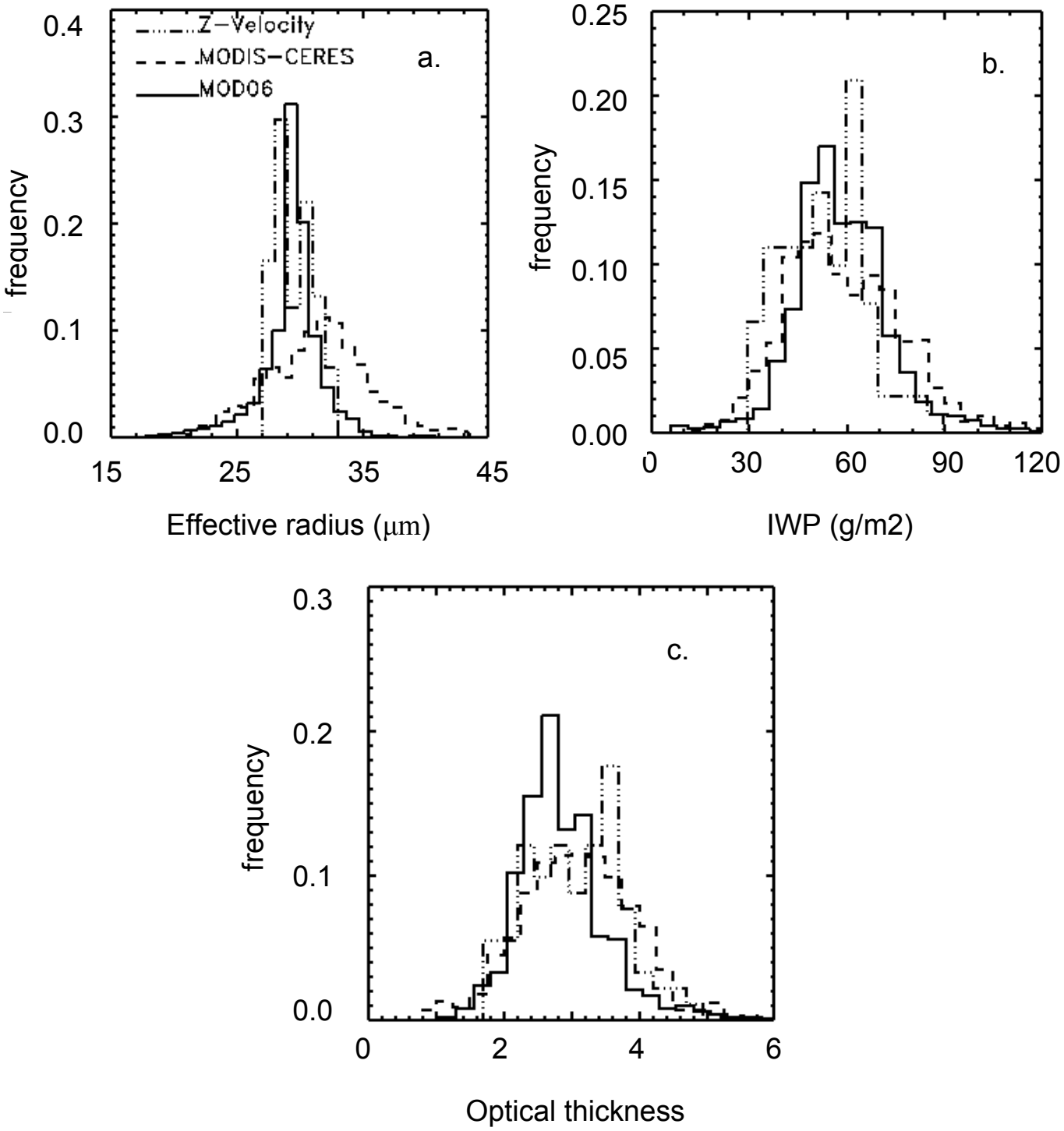

Figure 3. Comparison among cloud properties retrieved by the Z-Velocity algorithm applied to MMCR data collected at the SGP site, the MOD06 cloud properties, and the MODIS-CERES cloud properties retrieved using data collected on 6 March 2001 from within the rectangular region shown in Figure 2. a) shows effective particle radius, b) shows the ice water path and c) shows the optical thickness

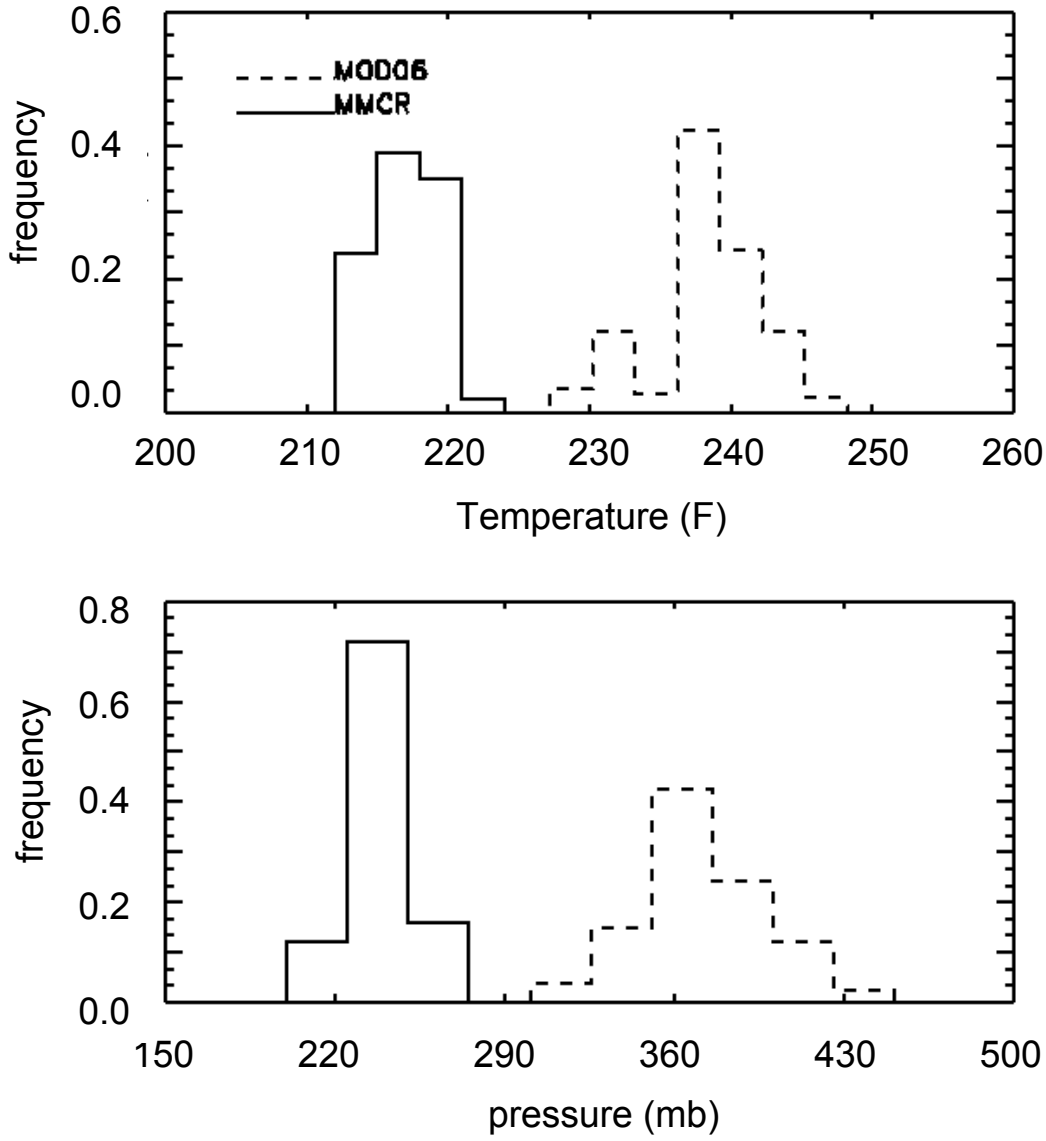

Figure 4. Comparison between cloud top (a) temperature and (b) pressure measured by the MMCR and local radiosonde data and that reported in the MOD06 product.

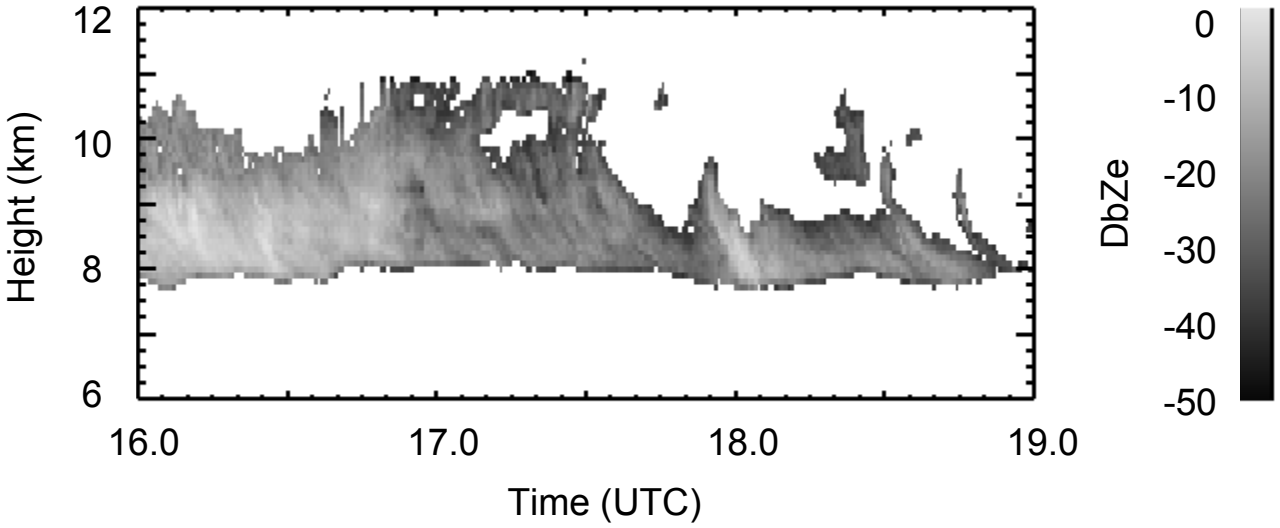

Figure 5. MMCR height-time cross section of radar reflectivity factor observed on 22 March 2001 at the ARM SGP site.

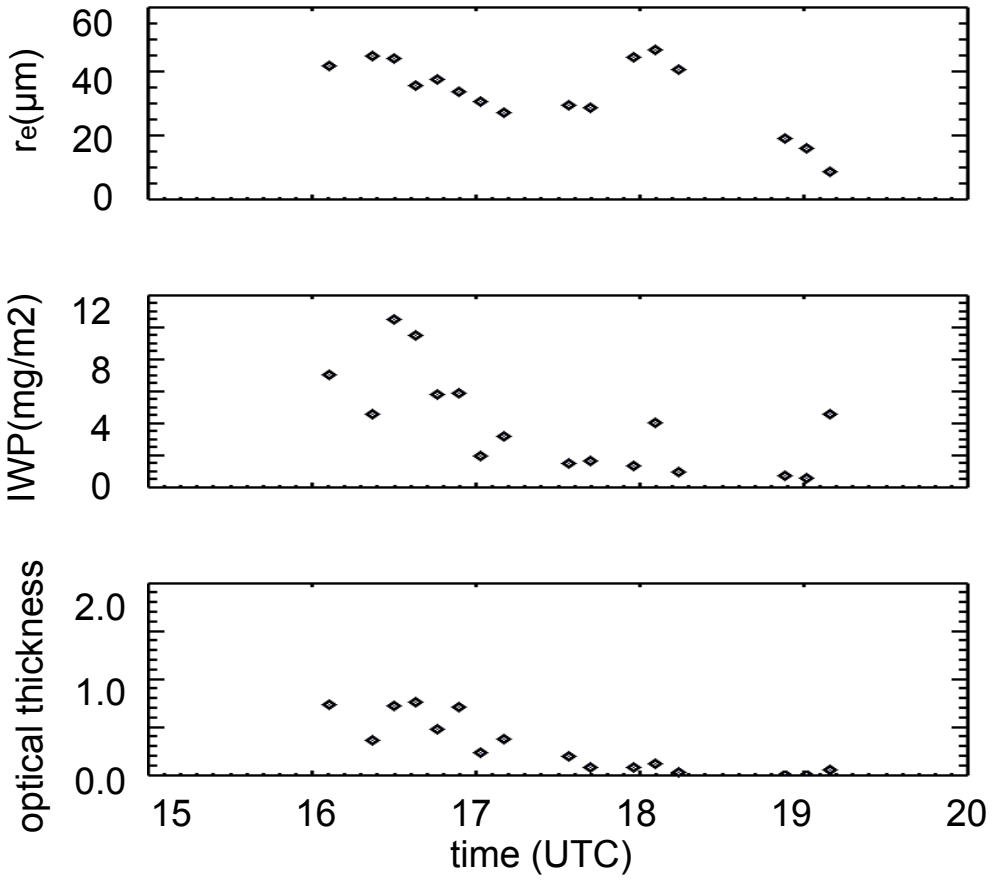

Figure 6. Layer-averaged cloud properties retrieved by the Z-Radiance algorithm using data collected on 22 March 2001.

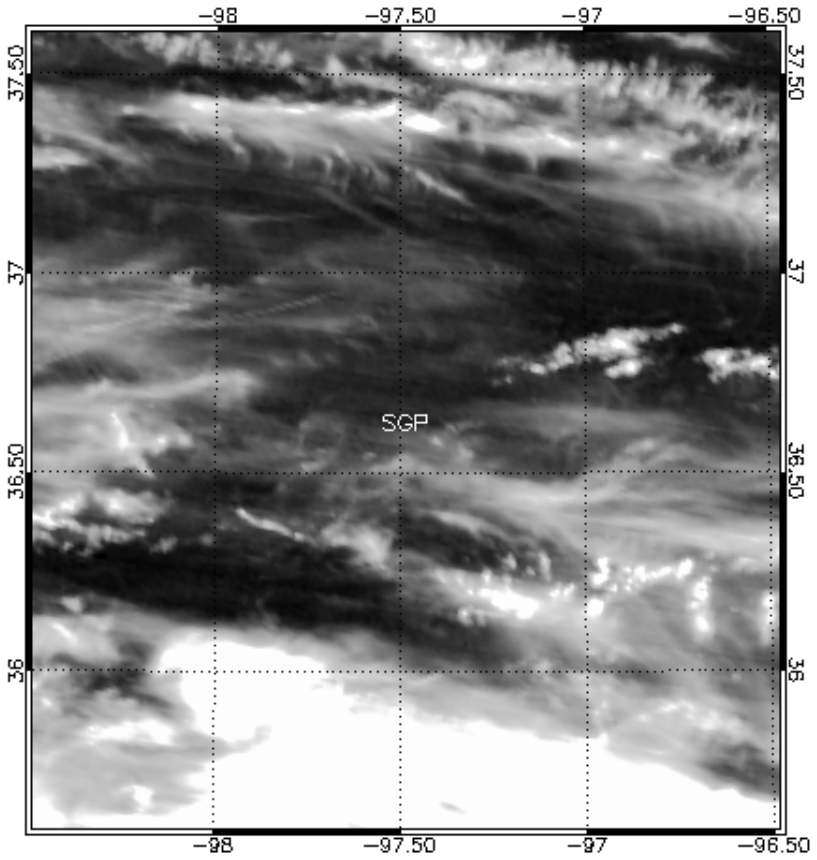

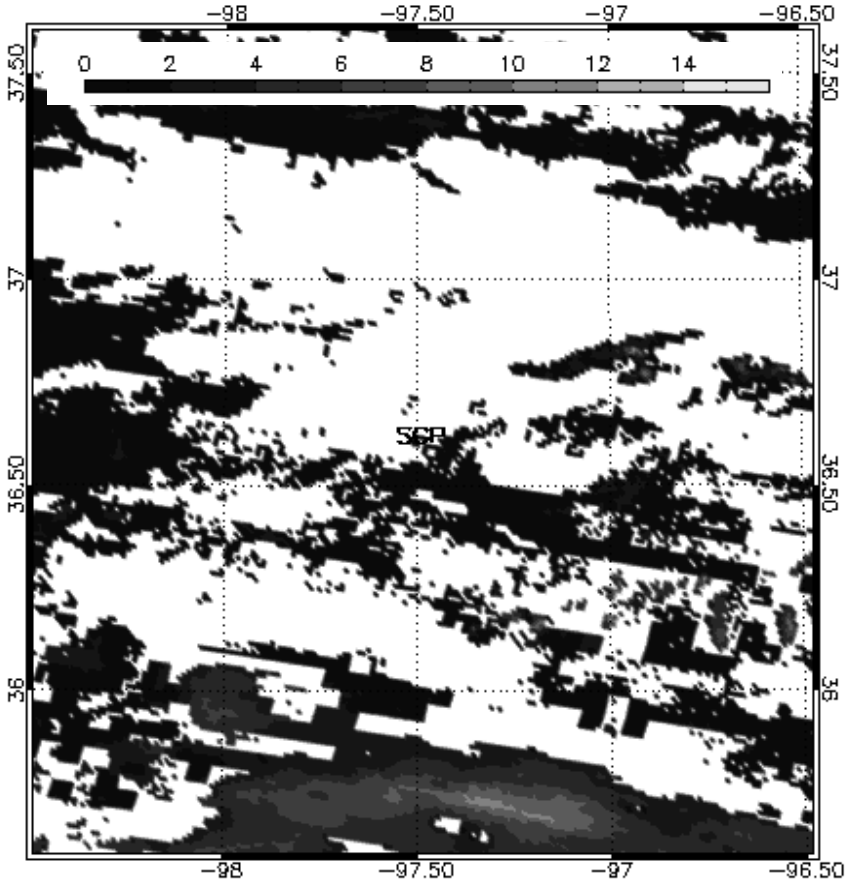

Figure 7. (a) MODIS 1.38 micro
imagery collected at 1735 UTC
on 22 March 2001 over the ARM
SGP site and (b) MOD06 optical
thickness coincident with the fiel
observed in (a).

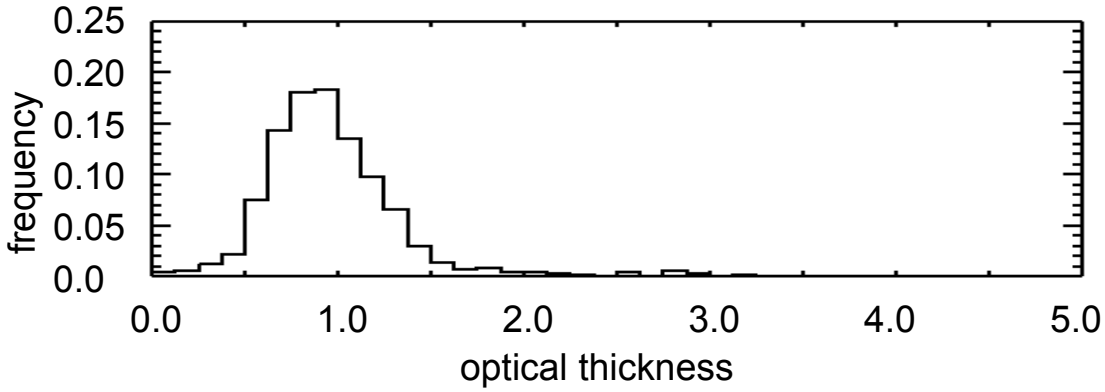

Figure 8. Frequency distribution of optical depth from the MOD06 data in the vicinity of the ARM site on 22 March 2001.

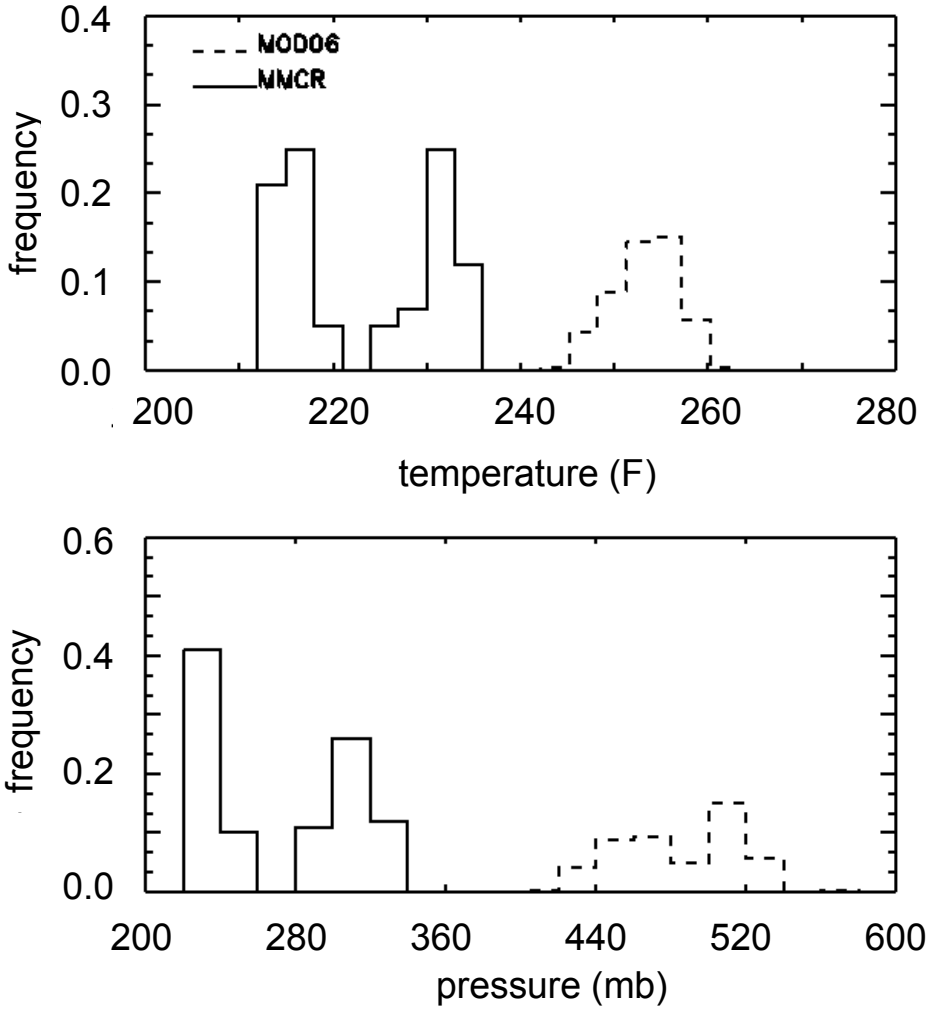

Figure 9. Comparison of cloud top temperature and pressure reported in the MOD06 product with observations

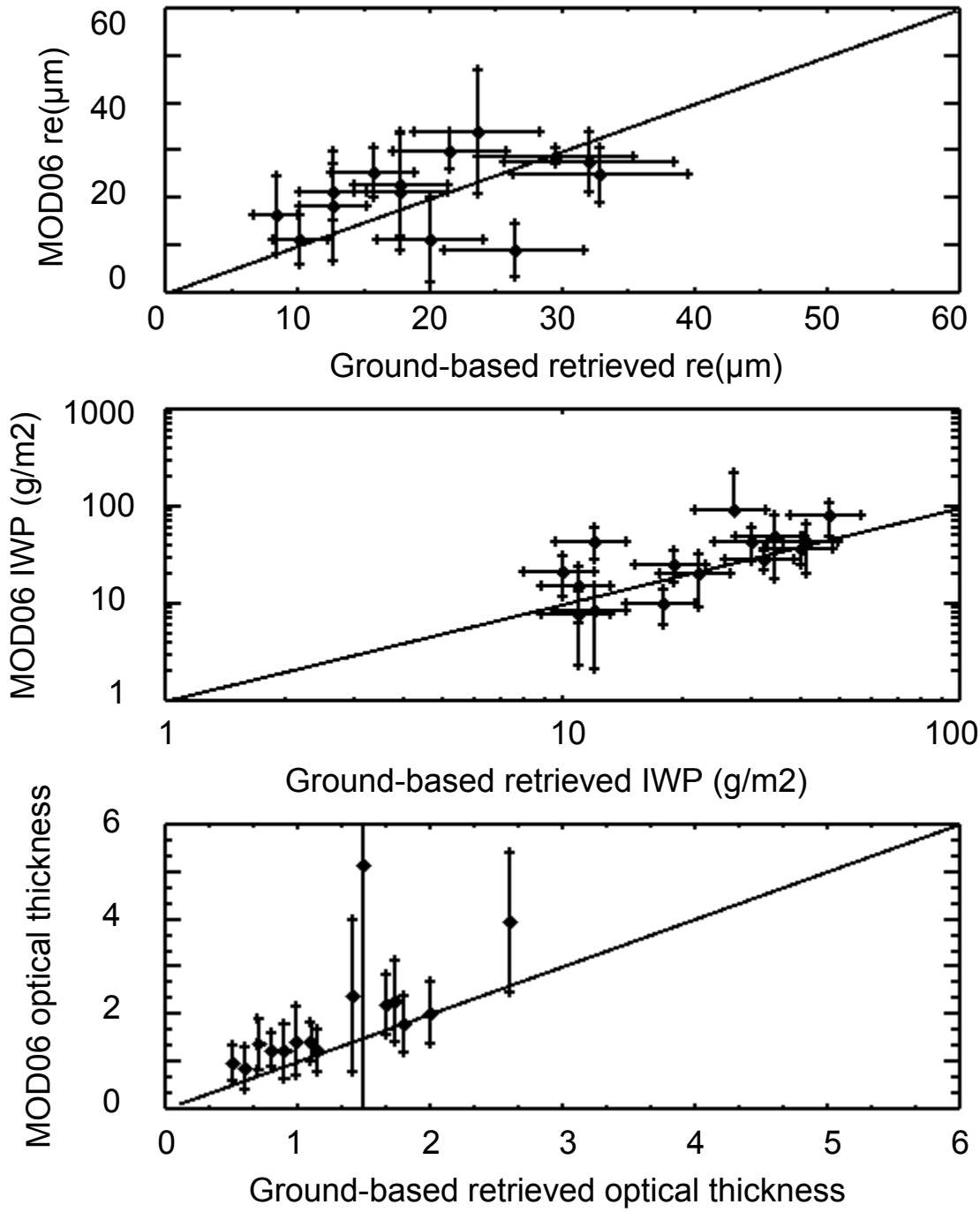

Figure 10. Comparison of cirrus properties from the Z-Radiance algorithm and coincident cloud properties reported in the MOD06 product.

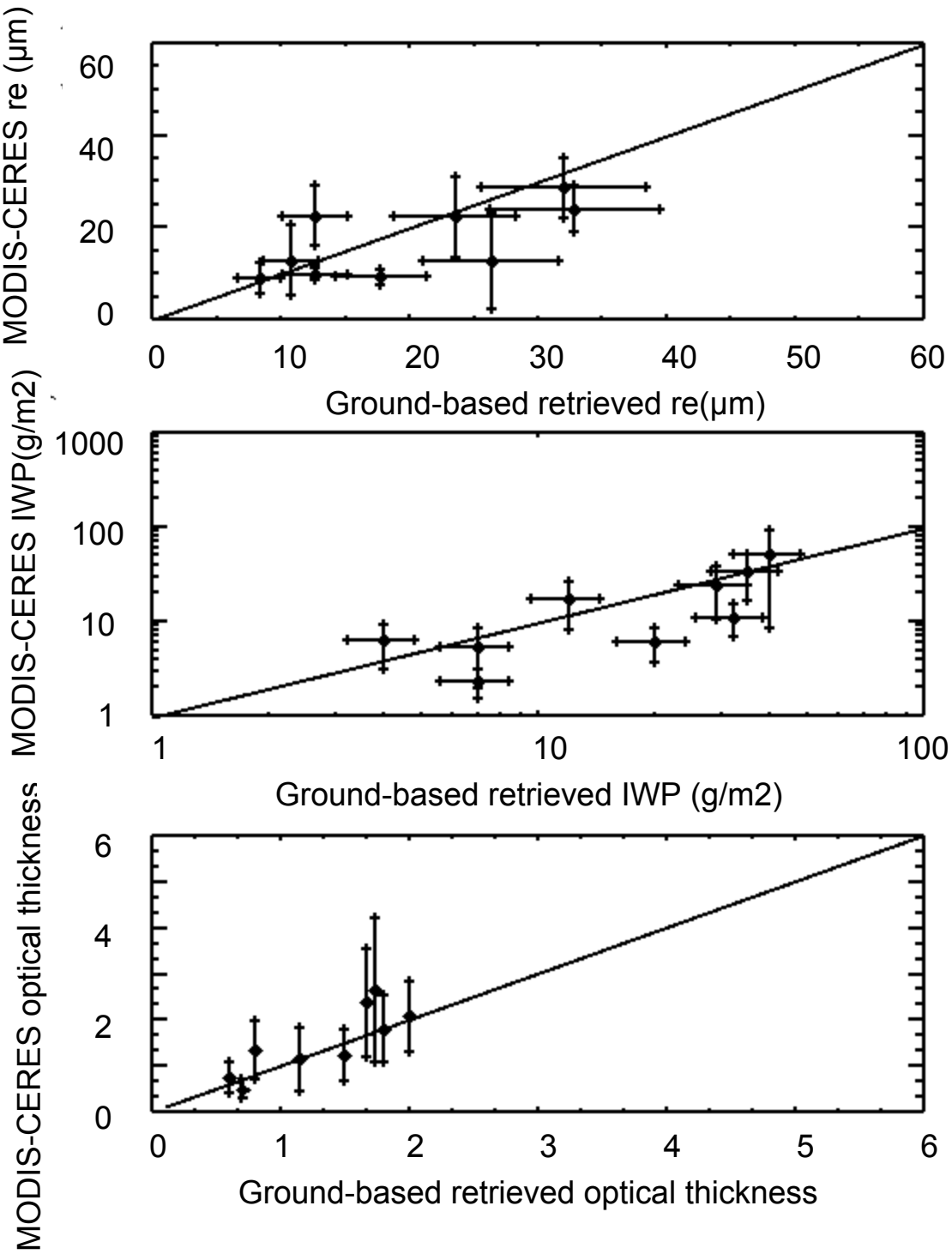

Figure 11. As in Figure 12 except the MODIS-CERES data is compared with the Z-Radiance results.

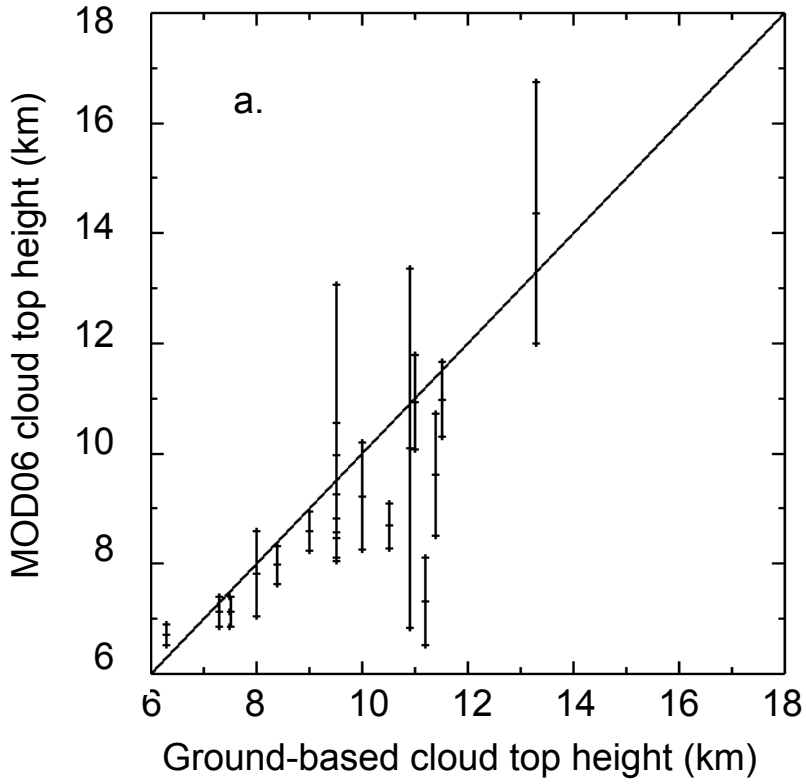

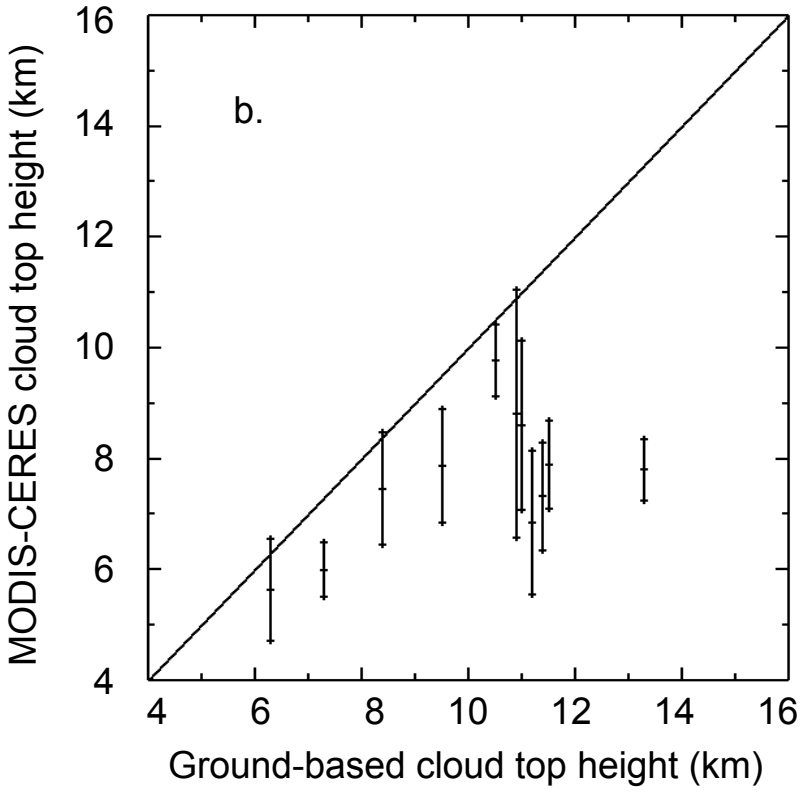

Figure 12. Comparison of cloud top heights reported by (a) the MOD06 product and (b) the MODIS-CERES products with observations at the ARM SGP site.

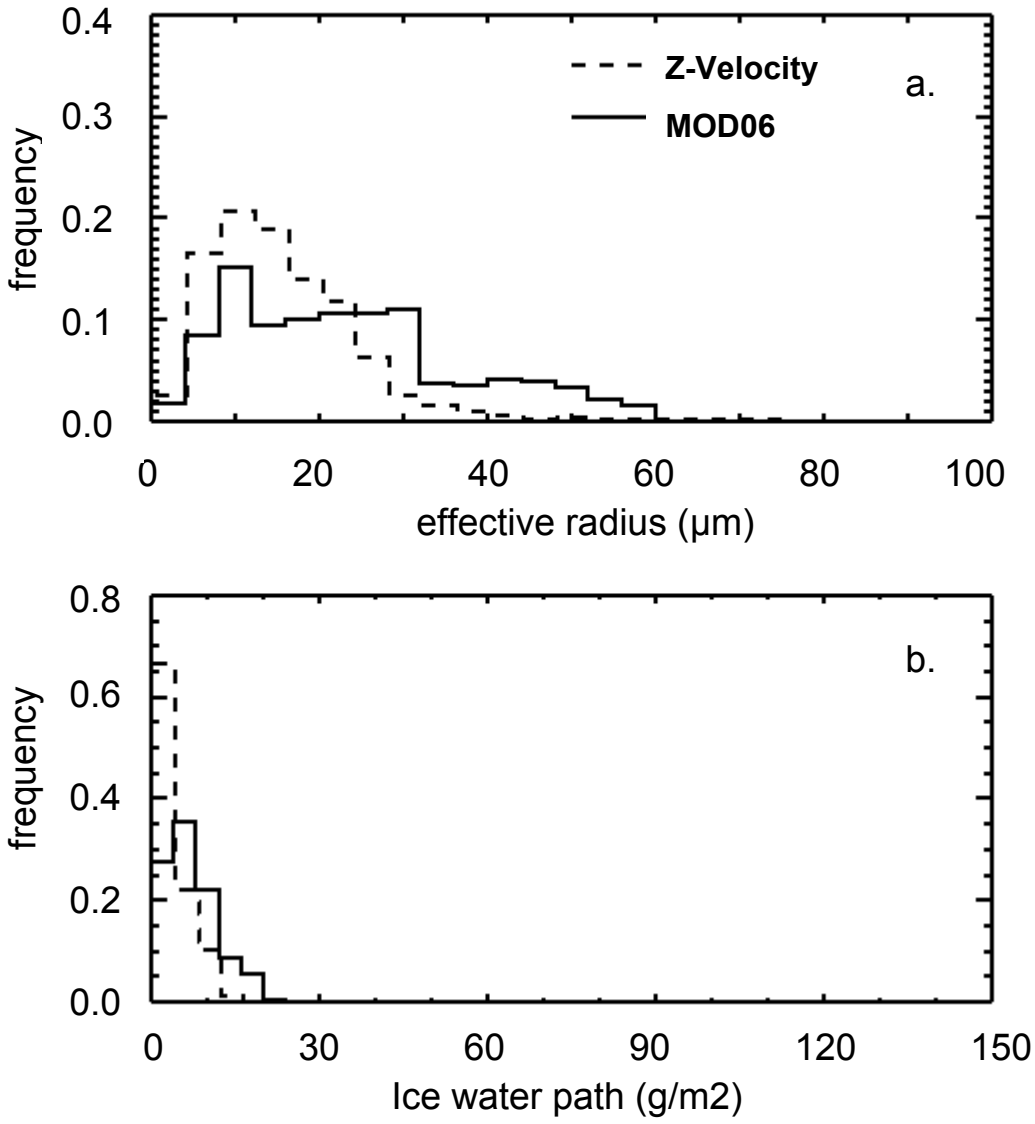

Figure 13. Comparison of the frequency distributions of effective radius (a) and ice water path (b) for cirrus with optical depths less than 0.5. The MOD06 properties are derived from a 100x100 km region centered on the ARM site for the period beginning in March 2000 and extending to July 2001. The Z-Radiance statistics are derived from cirrus clouds observed during this time period.

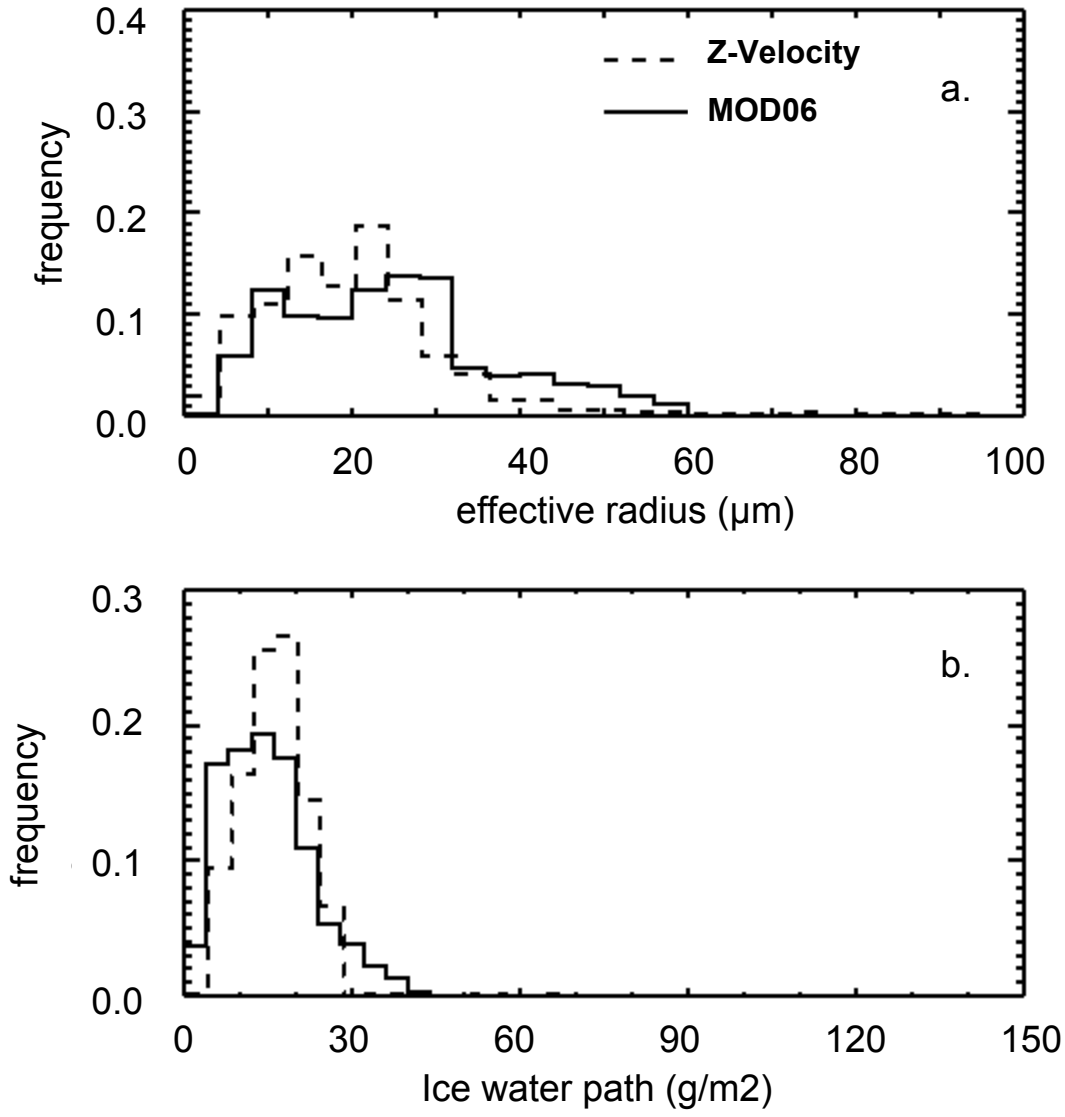

Figure 14. As in Figure 13 except for optical depths between 0.5 and 1.0

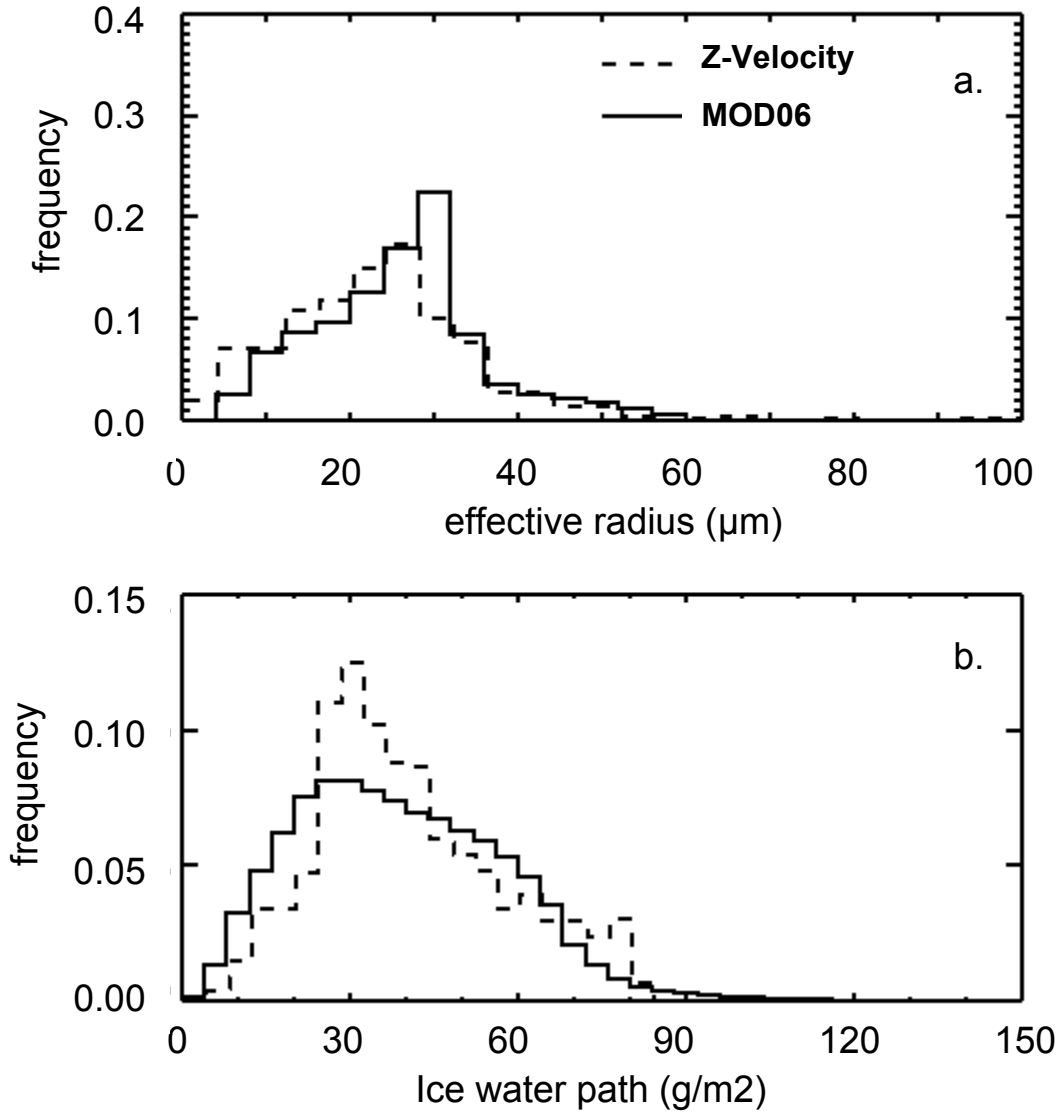

Figure 15. As in Figure 13 except for optical depths between 1.0 and 3.0

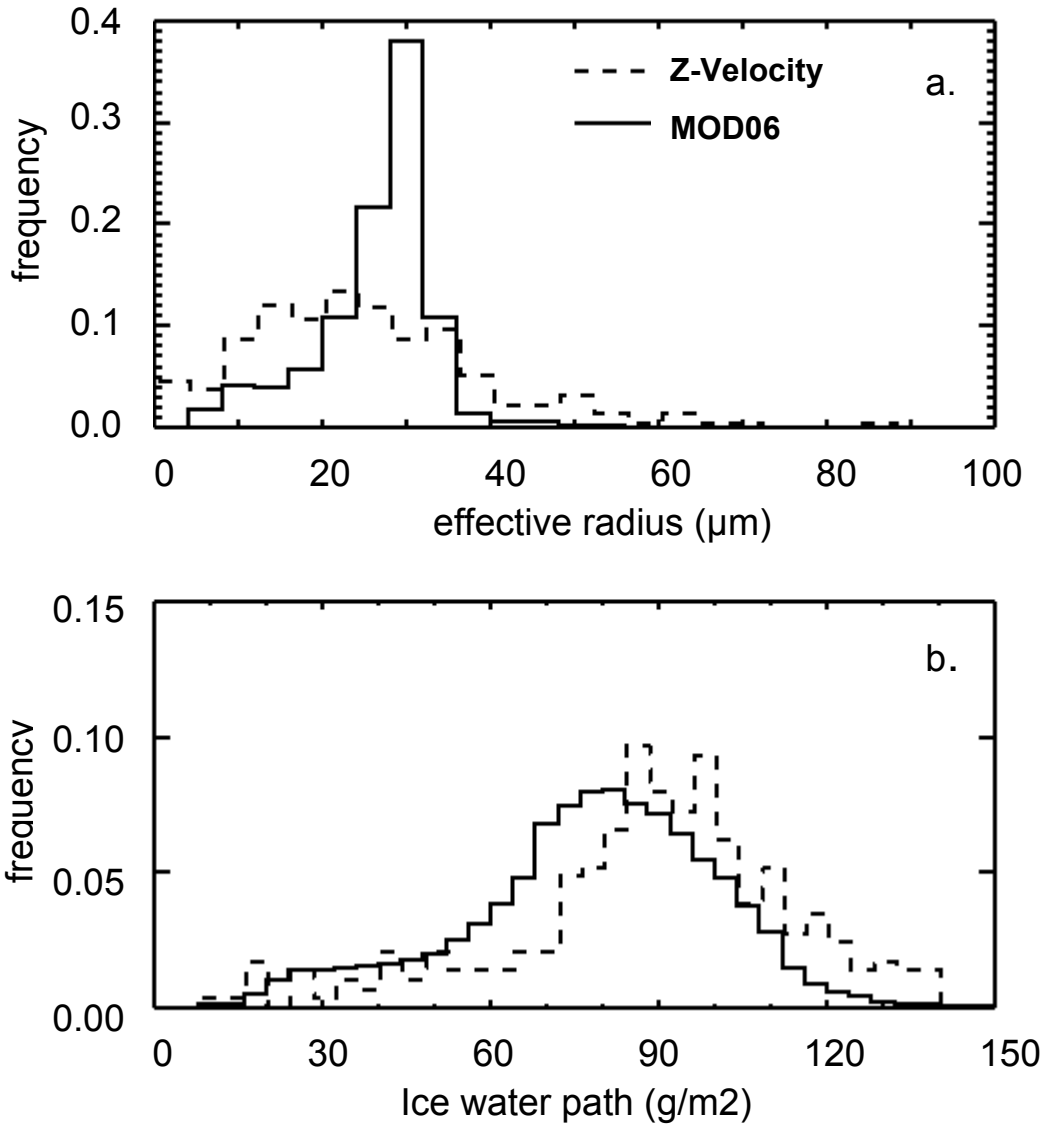

Figure 16. As in Figure 13 except for optical depths between 3.0 and 5.0

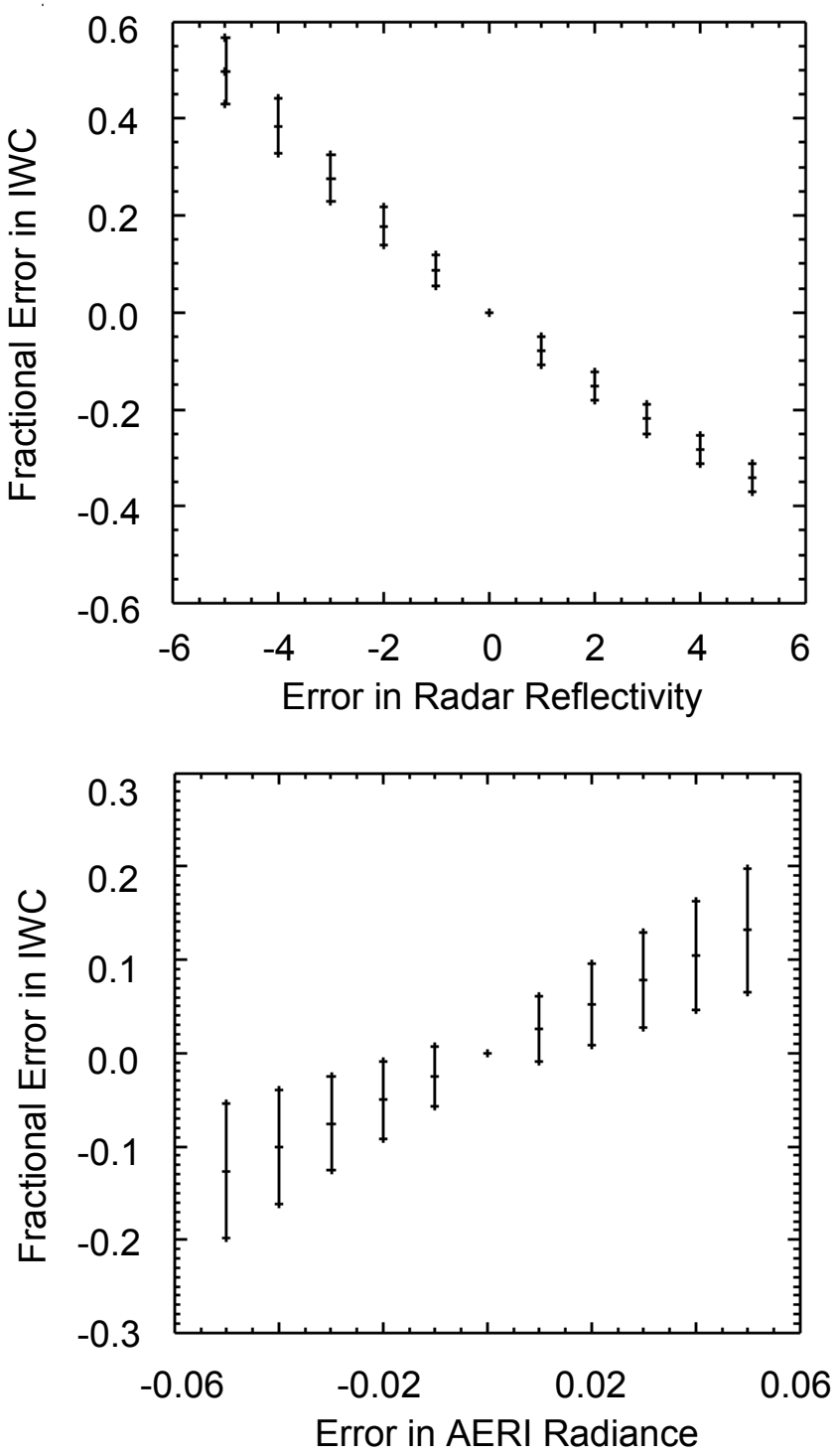

Figure A1. Sensitivity of the IWC retrieved by the Z-Radiance algorithm due to error in the input data.

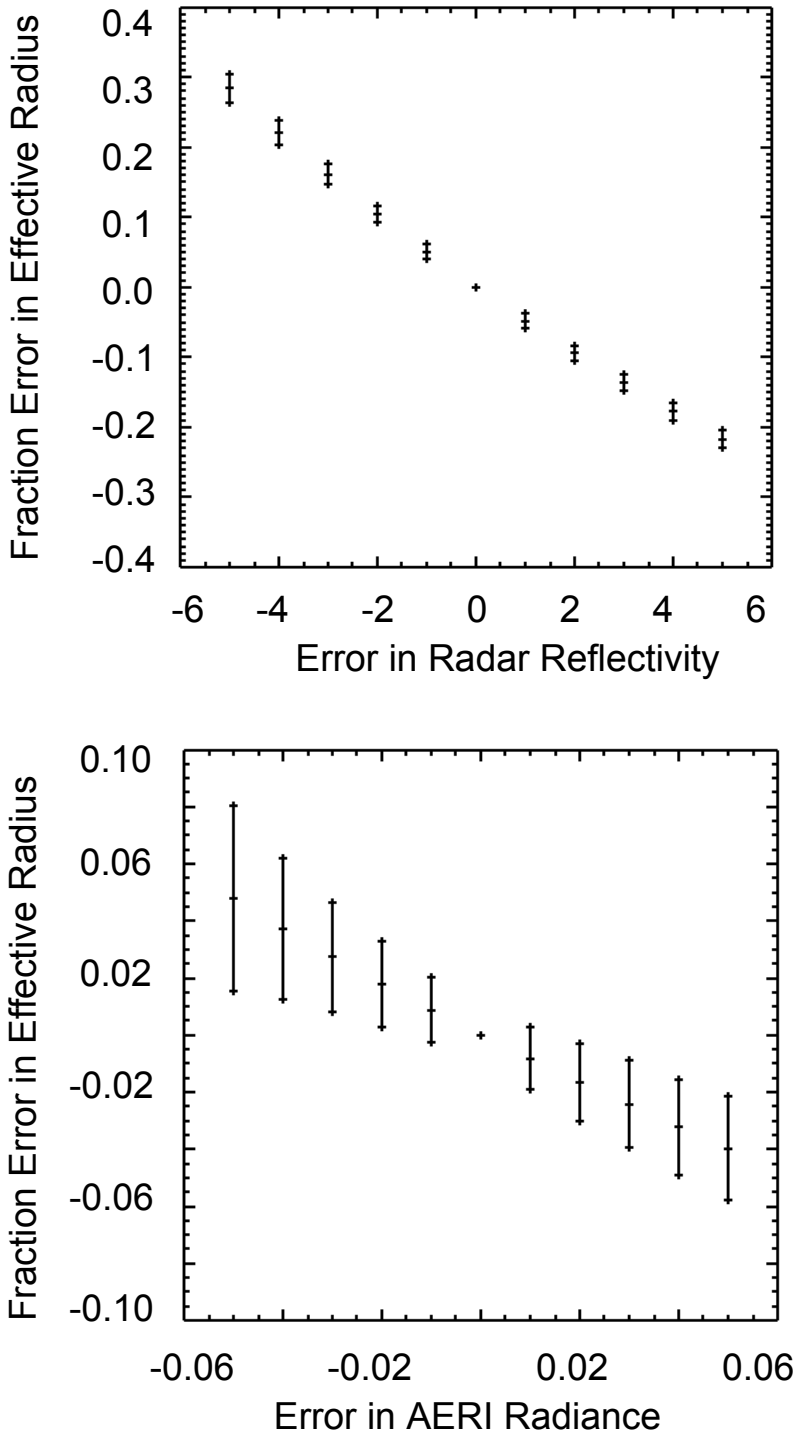

Figure A2. Sensitivity of the effective radius retrieved by the Z-Radiance algorithm due to error in the input data.

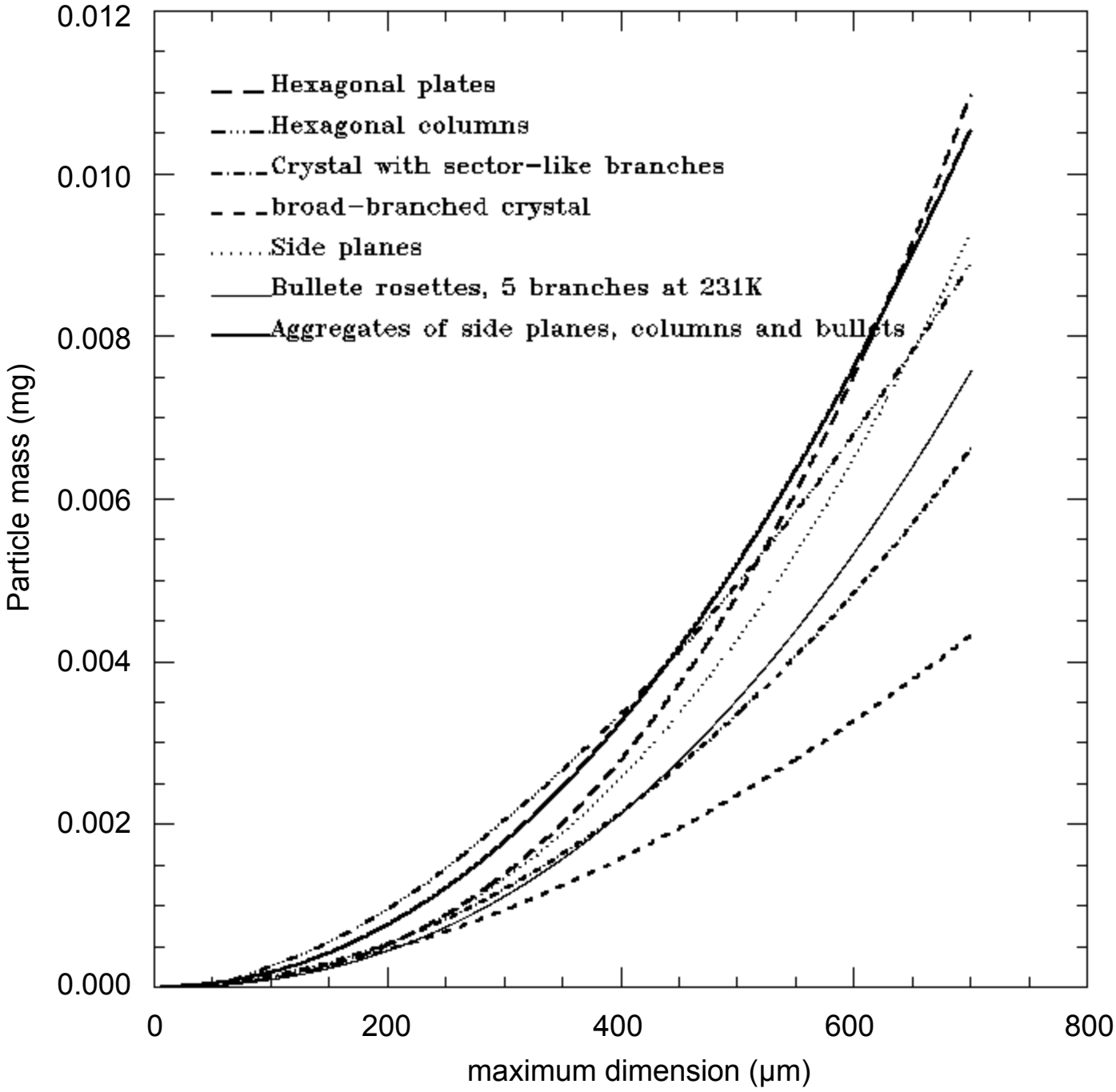

Figure A3. Mass-dimensional relationships used in the calculation of IWC from aircraft data.

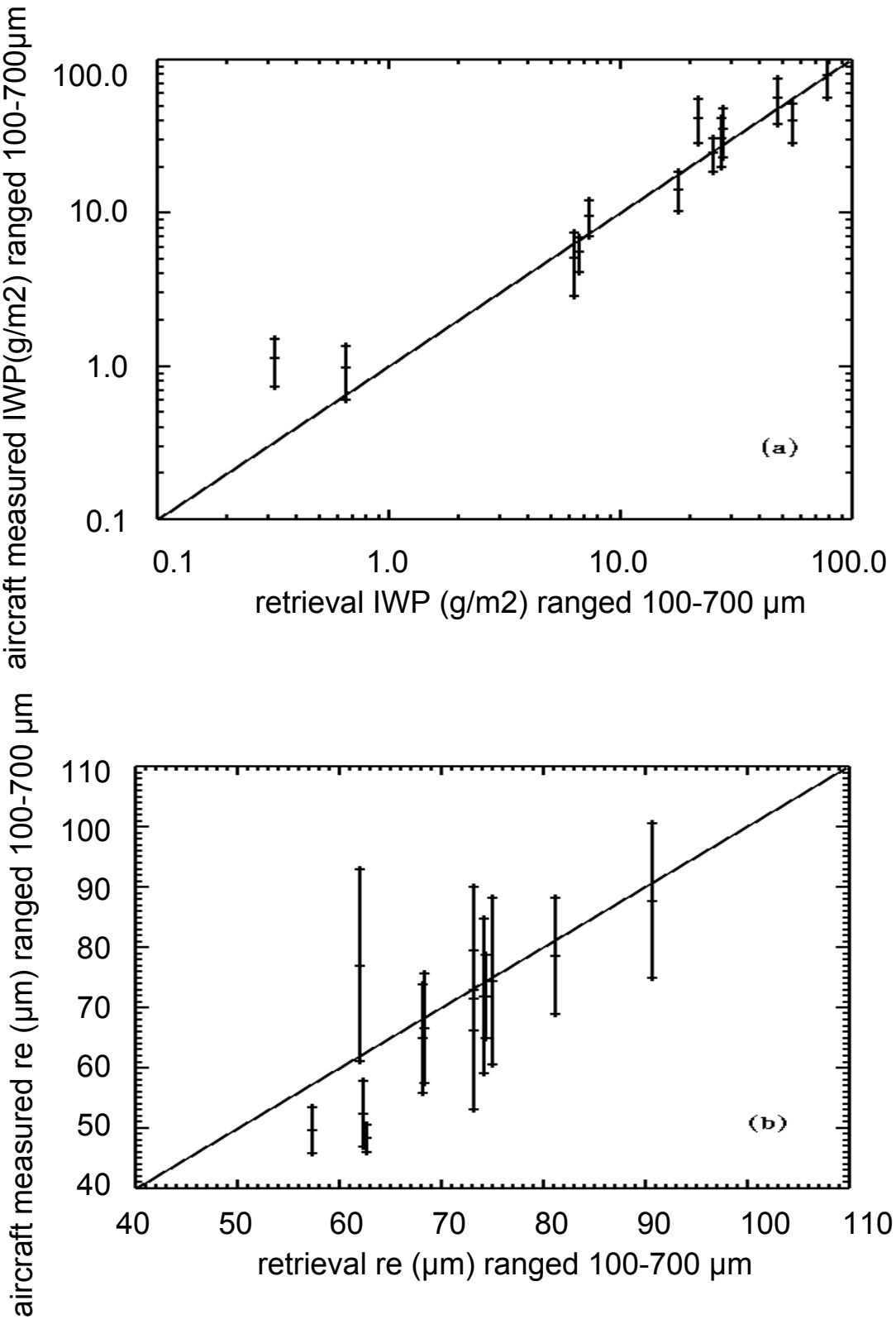

Figure A4. Comparison of aircraft-observed IWP and effective radius with retrieved values from the surface instruments. Due to limitations in the 2dc instrument, the observed and retrieved size distributions are integrated only over the 100-700 micron particle size range.

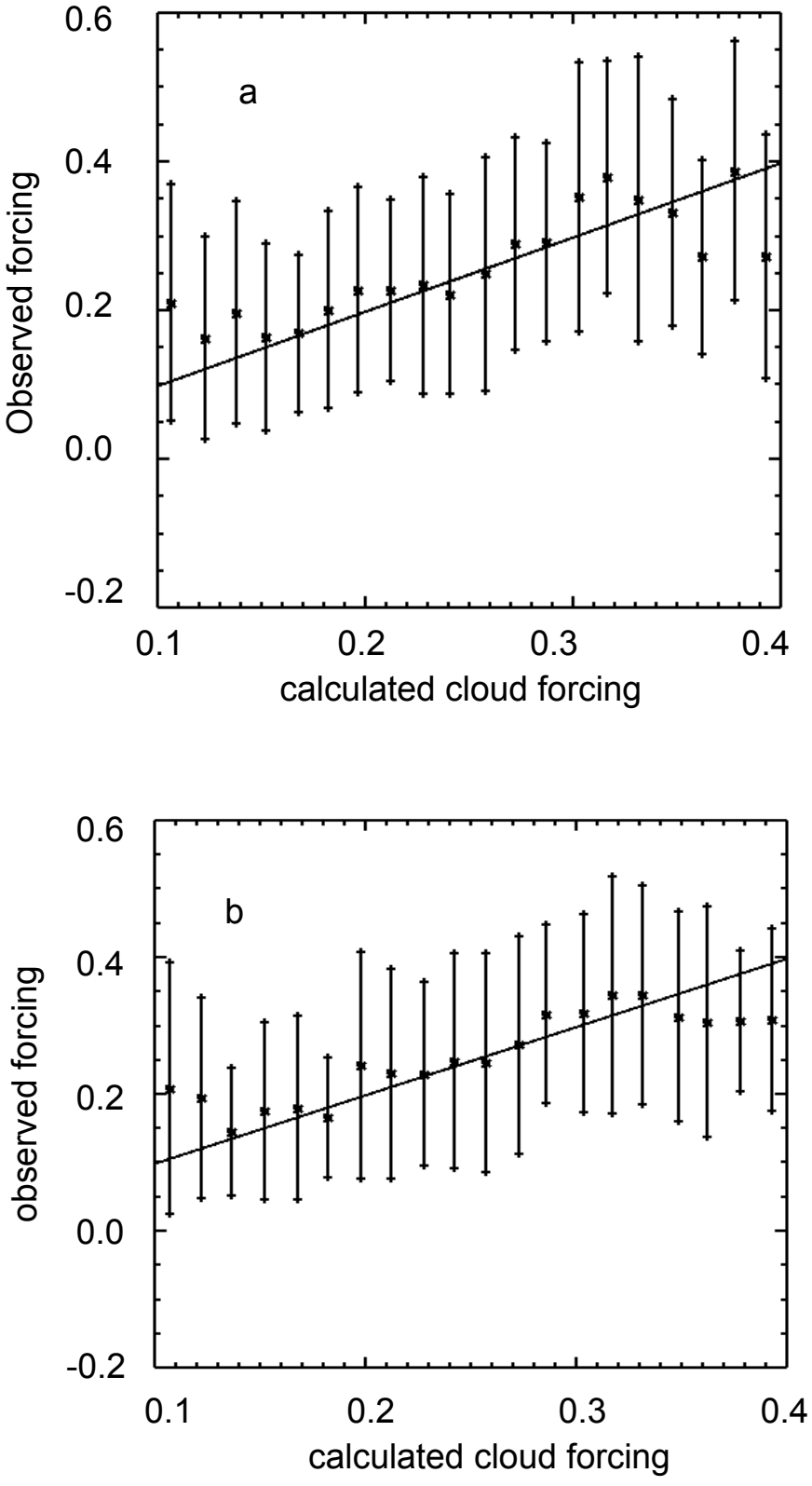

Figure A.5 Comparison between calculated and observed downwelling solar fluxes at the surface expressed in terms of the fraction of the downwelling solar flux removed by cloud. (a) solar forcing calculated from Mace98 algorithm, (b) solar forcing calculated from the improved reflectivity-radiance algorithm.

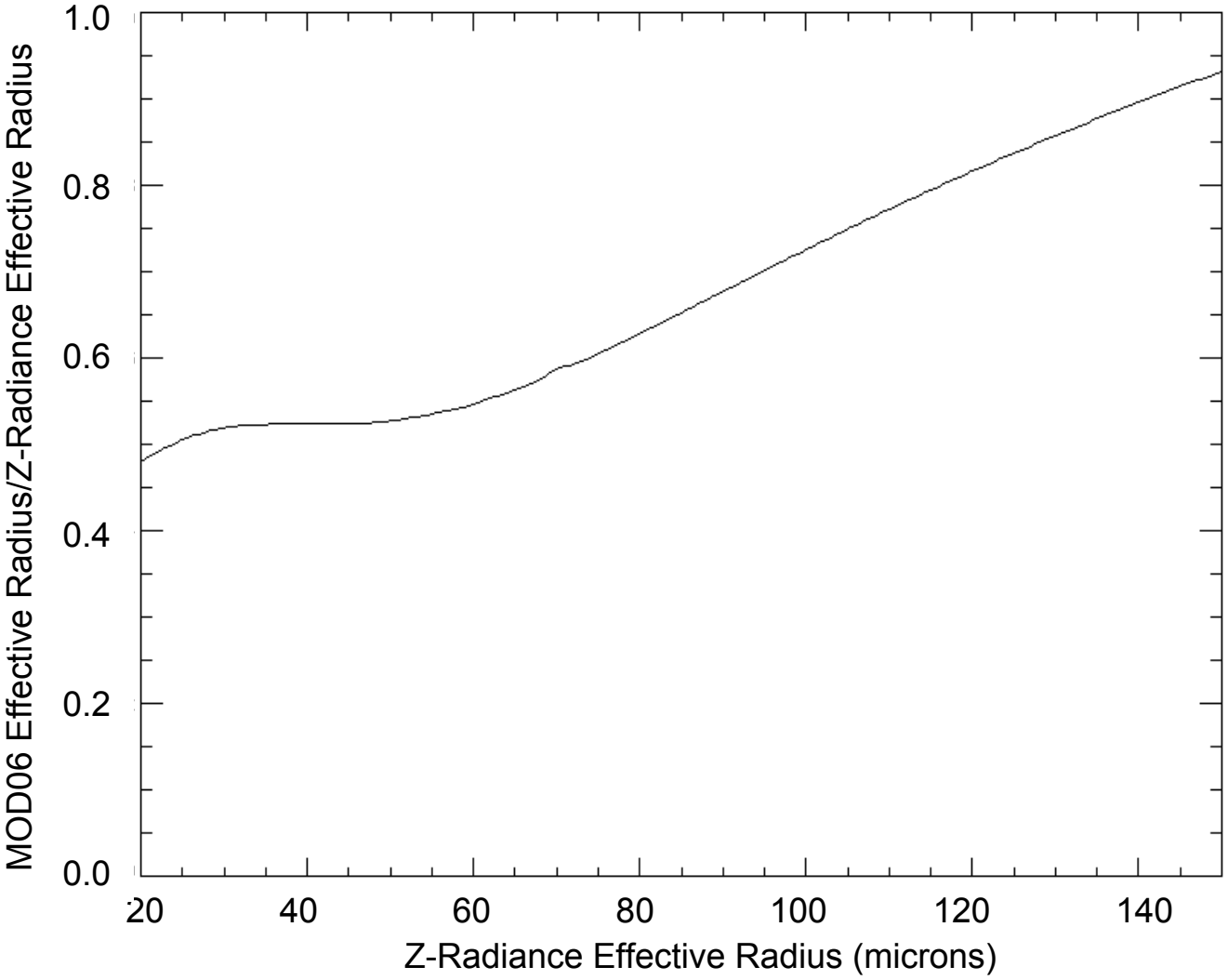

Figure B1. Ratio of the effective radius definition used in the MOD06 algorithm with that used in the Z-Radiance algorithm as a function of the Z-Radiance effective radius.